U.S. Department
of Transportation
**National Highway
Traffic Safety
Administration**

NHTSA

DOT HS 812 641

May 2019

Lower Leg Biofidelity Corridors For Heel Impact

DISCLAIMER

This publication is distributed by the U.S. Department of Transportation, National Highway Traffic Safety Administration, in the interest of information exchange. The opinions, findings, and conclusions expressed in this publication are those of the authors and not necessarily those of the Department of Transportation or the National Highway Traffic Safety Administration. The United States Government assumes no liability for its contents or use thereof. If trade names, manufacturers' names, or specific products are mentioned, it is because they are considered essential to the object of the publication and should not be construed as an endorsement. The United States Government does not endorse products or manufacturers.

Suggest APA Format Citation;

Forman, J. L., Crandall, J. R., & Roberts, C. W. (2019, May). *Lower leg biofidelity corridors for heel impac*t (Report No. DOT HS 812 641). Washington, DC: National Highway Traffic Safety Administration.

REPORT DOCUMENTATION PAGE

Form Approved
OMB No.0704-0188

1. AGENCY USE ONLY (Leave blank)	2. REPORT DATE	3. REPORT TYPE AND DATES COVERED
	May 2019	

4. TITLE AND SUBTITLE	5. FUNDING NUMBERS
Lower Leg Biofidelity Corridors for Heel Impact	Contract Number DTNH2215D00022/0003 Task 4
6. AUTHORS	
Jason L. Forman, Jeff R. Crandall, Carolyn W. Roberts	
7. PERFORMING ORGANIZATION NAME AND ADDRESS	8. PERFORMING ORGANIZATION REPORT NUMBER
University of Virginia Center for Applied Biomechanics 4040 Lewis and Clark Dr. Charlottesville, VA 22911	
9. SPONSORING/MONITORING AGENCY NAME(S) AND ADDRESS(ES)	10. SPONSORING/MONITORING AGENCY REPORT NUMBER
National Highway Traffic Safety Administration 1200 New Jersey Avenue SE. Washington, DC 20590	DOT HS 812 641
11. SUPPLEMENTARY NOTES	
12a. DISTRIBUTION/AVAILABILITY STATEMENT	12b. DISTRIBUTION CODE
This document is available to the public through the National Technical Information Service, www.ntis.gov.	

13. ABSTRACT

This report describes the methodology and results of development of biofidelity response corridors based on data for axial loading through the heel of 12 small female post mortem human surrogates (PMHS) lower extremities, and 2 additional small female PMHS. These biofidelity response corridors were based on anticipated measurement capabilities of typical ATDs, and include metrics such as internal tibia and fibula axial load, external footplate axial load, knee axial load, and footplate displacement.

Methodologies include initial data treatment, development of coordinate systems, transformation of internal load cell measurements from PMHS to an anatomic coordinate system analogous to a 5th percentile female ATD, load cell compensation for the footplate load cell, scaling techniques, data inclusion analysis, and corridor development techniques. An initial examination was performed for the footplate displacement and all axial force traces using the ISO rating method to determine if any individual trace was an outlier, or if there was a systematic difference between the shod condition and the barefoot condition. The combined dataset corridors are based on 12 tests, shod corridors are based on 7 tests, and barefoot corridors are based on 5 tests. For time-history corridors, footplate axial displacement, footplate load cell forces (raw and mass compensated), total cross sectional axial force from the tibia and fibula load cells, tibia load cell axial force, fibula load cell axial force, and knee axial load are reported. For cross plotted footplate displacement corridors, mass-compensated footplate axial load, total cross sectional axial force from the tibia and fibula load cells, tibia load cell axial force, fibula load cell axial force, and knee axial load are reported. A scaling analysis was also performed, and found leg length to be a better metric for scaling than total height. The same time-history and cross plotted footplate displacement corridors were developed with leg length based scaled data. Overall, it was found that the shod corridors developed were narrower than either the combined dataset corridors or the barefoot corridors. Additionally, corridors developed with data scaled by leg-length were narrower than those developed using unscaled data. Shod, scaled corridors are recommended for use in 5th female ATD biofidelity evaluations.

14. SUBJECT TERMS	15. NUMBER OF PAGES
	64
	16. PRICE CODE

17. SECURITY CLASSIFICATION OF REPORT	18. SECURITY CLASSIFICATION OF THIS PAGE	19. SECURITY CLASSIFICATION OF ABSTRACT	20. LIMITATION OF ABSTRACT
Unclassified	Unclassified	Unclassified	

Table of Contents

Executive Summary

This report includes details on the methodology and results of Task 4 under NHTSA contract number DTNH2215D00022/0003. Details are given about the development of biofidelity response corridors based on data for axial loading through the heel of 12 small female post mortem human surrogates (PMHS) lower extremities tested under NHTSA contract number DTNH2215D00022/0003, and two additional small female PMHS, tested in the same conditions under NHTSA cooperative agreement No. DTNH22-09-H-00247. These biofidelity response corridors were based on the anticipated measurement capabilities of typical ATDs, and include metrics such as internal tibia and fibula axial load, and external footplate axial load, knee axial load, and footplate displacement.

Methodologies described include initial data treatment, development of coordinate systems, transformation of internal load cell measurements from PMHS to an anatomic coordinate system analogous to a 5th percentile female ATD, load cell compensation for the footplate load cell, scaling techniques, data inclusion analysis, and corridor development techniques. An initial examination was performed for the footplate displacement and all axial force traces using the ISO rating method to determine if any individual trace was an outlier, or if there was a systematic difference between the shod condition and the barefoot condition. Limited differences were found using the ISO rating method, so individual corridors were developed including all tests, only shod condition tests, and only barefoot condition tests. During initial corridor creation, it was noticed that Tests 3 and 15 exhibited a different response shape compared to the other tests (due to differences in kinematics) changing the shape of the corridors, making them wider. The fact that these tests resulted in different kinematics and an artefactual injury inside a potting cup, lead to its removal these two tests in all of the developed corridors. Therefore, the combined dataset corridors are based on 12 tests, shod corridors are based on 7 tests, and barefoot corridors are based on 5 tests. For time-history corridors, footplate axial displacement, footplate load cell forces (raw and mass compensated), total cross sectional axial force from the tibia and fibula load cells, tibia load cell axial force, fibula load cell axial force, and knee axial load are reported. For cross plotted footplate displacement corridors, mass-compensated footplate axial load, total cross sectional axial force from the tibia and fibula load cells, tibia load cell axial force, fibula load cell axial force, and knee axial load are reported. A scaling analysis was also performed, and found leg length to be a better metric for scaling than total height. The same time-history and cross plotted footplate displacement corridors were developed with leg length based scaled data.

Overall, it was found that the shod corridors developed were narrower than either the combined dataset corridors or the barefoot corridors. Additionally, corridors developed with data scaled by leg-length were narrower than those developed using unscaled data. Shod, scaled corridors are recommended for use in 5th female ATD biofidelity evaluation.

Introduction

Six matched pairs of female PMHS lower extremities were tested under an axial impact loading condition to develop response corridors at University of Virginia Center for Applied Biomechanics (UVA CAB). This test series was conducted in support of NHTSA's effort to establish biofidelity targets of a 5th female ATD lower extremity. Both shod and unshod configurations were considered (Table 1). Each pair of specimens were tested in the shod condition for one leg and in the unshod condition for the other one. The shod aspect was chosen randomly (constrained so that half of each aspect were tested shod). Shoes used in this test were women's low heel, dress, black, oxford shoe with standardized design by the U.S. Military Standard MIL-S-21711E. This shoe is also designated for use with the Hybrid III 5th percentile female ATD.

Table 1: Test matrix

Test number	Test Name	Subject ID*	Measured Impact Speed (m/s)	Ballistic Mass (kg)	Test Condition
1	UVAB015	820-R	2.97	28.4	Barefoot
2	UVAB016	820-L	2.99	28.4	MIL-spec shoe
3	UVAB017	822-L	2.83	28.4	MIL-spec shoe
4	UVAB018	822-R	2.92	28.4	Barefoot
5	UVAB019	840-R	2.77	28.4	MIL-spec shoe
6	UVAB020	840-L	2.9	28.4	Barefoot
7	UVAB021	841-L	2.92	28.4	Barefoot
8	UVAB022	841-R	2.98	28.4	MIL-spec shoe
9	UVAB023	844-R	2.93	28.4	Barefoot
10	UVAB024	844-L	3.02	28.4	MIL-spec shoe
11	UVAB025	845-L	2.99	28.4	Barefoot
12	UVAB026	845-R	2.98	28.4	MIL-spec shoe

* R-right leg; L-left leg

A schematic of the test setup can be found in Figure 1, below. Further details about test setup, instrumentation, PMHS details, data collection methodologies, injury, and raw data results can be found in the corresponding test report, *Lower Leg Biofidelity and Injury Risk Assessment*, which corresponds to Task 3 of the same project.

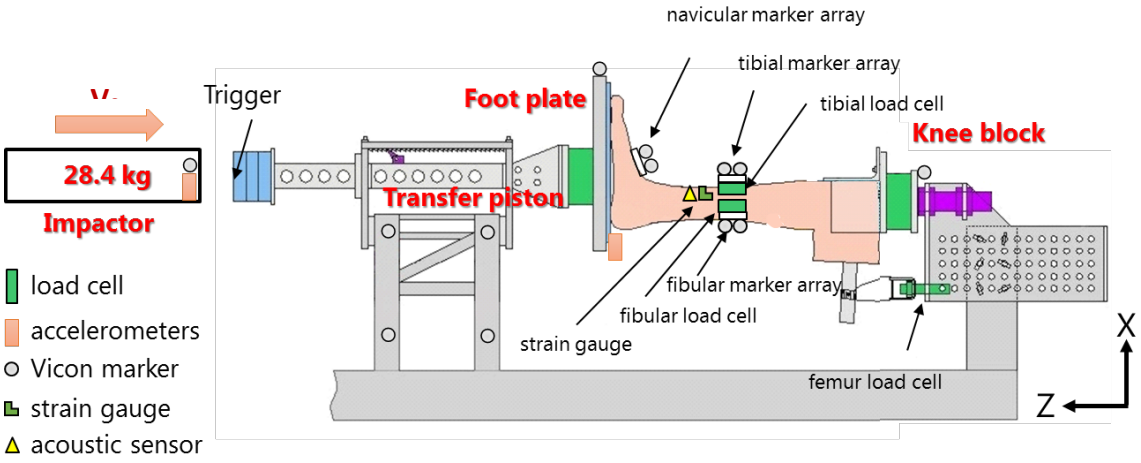

Figure 1: Axial Impact Test Set-up

This document contains details on post-processing of the force and kinematic data, as well as development of biofidelity corridors, and description of how these biofidelity corridors should be used when evaluating ATDs.

Data Analysis

Initial Data Processing

Data included for all post processing and biofidelity corridor creation techniques described below are the six pairs of small female PMHS tested in axial loading, and one pair of small female PMHS tested in 2013 under the same loading conditions. The data from the small PMHS tests in 2013 were tested with the same equipment in the same boundary condition. All recorded data were filtered according to SAE J211, debiased, and then cropped to -98 ms to 150 ms, to include both the initial loading and unloading of the legs, (note that: t= 0 ms was time of impact). While all data plotted against time was analyzed at 10,000 Hz, the sampling frequency used in Sliceware from testing, data plotted against displacement was down-sampled to 500 Hz, to match the sampling frequency from VICON from testing and to improve compatibility with the corridor creation algorithm. Additionally, Vicon data was up-sampled to 10,000 Hz. All corridors were formed with both 500 Hz and 10,000 Hz data, to determine which data frequency was best for corridor formation. Data plotted against footplate displacement were cropped at the time of maximum footplate displacement.

Anatomic Coordinate Systems

Force and moment data recorded by the internal tibia and fibula load cells needed to be transformed to a common coordinate system, to compare measured forces between specimens in the same anatomic location. Load cell placement along the length of the tibia and fibula was different for each specimen, given differences in leg length and tibia and fibula width and spacing for each PMHS. This was because the load cells were implanted with a goal to not change the natural alignment of the tibia and fibula; changing natural alignment could introduce different loading distributions in the tibia and fibula. A combined tibia and fibula coordinate system was developed using anatomic landmarks on the tibia and the fibula. The goal in the creation of this coordinate system was to match the orientation of the forces measured in the PMHS anatomic coordinate system as closely as possible to the a 5th female ATD lower extremity load cell coordinate system.

Figure 1 depicts the points taken from CT scans of all tested specimens, and the points calculated to determine the PMHS anatomic coordinate system. All points in blue were taken directly from CT scans, while the green points and red and black lines were calculated. Two points were taken on the proximal tibia, the most medial and lateral points on the tibial plateau. A further two points were taken at the distal end of the tibia and fibula, the most medial point of the medial malleolus, and the most lateral point on the lateral malleolus. The midpoint of the medial and lateral points on the tibial plateau was calculated, as was the midpoint of the points taken from the medial and lateral malleolus. The origin of the anatomic coordinate system, point 7, was defined as the midpoint of the midpoints calculated from the malleoli (point 5) and the points on the tibial plateau (point 6).

The direction of the positive Z-axis was calculated by subtracting the midpoint calculated from the malleoli from the midpoint calculated from the points on the tibial plateau. This vector was normalized, and plotted to ensure that the positive Z-axis was always pointing distal. The positive Y-axis was calculated by averaging the vectors formed by subtracting the medial points from the lateral points. This vector was also normalized to give a Y-direction. For the left feet, this vector was multiplied by negative one to ensure the positive Y-axis was always pointing to the right-hand side of the specimen, to match the anatomic coordinate system. Y-axis directions were also plotted to ensure the sign convention was correct for all right and left tested specimens. The X-direction was calculated by taking the cross product of the normalized positive Y-axis and Z-axis vectors. Again, this data was plotted to ensure that the positive X-axis was pointing in the anterior direction for all tested specimens.

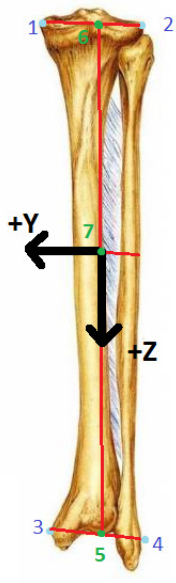

1	From CT: Most medial point on the tibial plateau
2	From CT: Most lateral point on the tibial plateau
3	From CT: Most medial point on the medial malleolus
4	From CT: Most lateral point on the lateral malleolus
5	Calculated: midpoint of the two malleoli
6	Calculated: midpoint of the medial and lateral points on the tibial plateau
7	Calculated: Origin of the anatomical coordinate system, located at the midpoint of points 5 and 6
+X	Anatomic positive X-axis, points out of the page and is calculated by taking the cross product of the positive Y- and Z-axes
+Y	Anatomic positive Y-axis, the direction is calculated by averaging the slopes of the lines that connect the medial and lateral malleolus and the most medial and most lateral points on the tibial plateau. The axis starts at the origin, and always points to the right-hand side of the body
+Z	Anatomic positive Z-axis, always points distal. Calculated by subtracting the midpoint of the medial and lateral malleolus (point 5) from the midpoint of the medial and lateral points on the tibial plateau (point 6)

Figure 2. Depiction of points and calculations required to form the anatomic coordinate system. The picture shows the locations of the points on the tibia and fibula (right), and the table gives descriptions as to how those points can be found (left).

Tibia and Fibula Load Cell Coordinate Systems

The internal tibia and fibula load cell coordinate systems were defined with the goal of matching them as closely as possible to the anatomic coordinate system; however, this was an approximation as the X and Y measurement axes in the internal load cells were not directly aligned with the anatomic coordinate systems when they were implanted in the specimens. Figure 2 depicts the points taken from CT scans, the calculated origin, and directions of the load cell coordinate systems for the tibia (top) and the fibula (bottom)

From all the CT scans, four points were taken from the tibia load cell: the proximal side screw hole, the distal side screw hole, the proximal posterior screw hole, and the proximal anterior screw hole. All points were defined as the center of each screw hole. The origin was calculated as the intersection of the line formed by subtracting the proximal side screw hole from the distal side screw hole and the line formed by subtracting the proximal anterior screw hole from the proximal posterior screw hole. This placed the origin at the center of the tibia load cell. The positive tibia load cell X-direction was defined by the normalized vector resulting from subtracting the proximal anterior screw hole from the proximal posterior screw hole. The positive tibia load cell Z-direction was calculated by normalizing the vector formed by subtracting the proximal side screw hole from the distal side screw hole. The positive tibia load cell Y-direction was calculated by taking the cross product of the positive normalized Z-vector and the positive normalized X-vector. As in the anatomic load cell, all directions for the tibia load cell coordinate system

were plotted, to ensure a right-handed coordinate system was formed for all legs, and that the positive Z-direction pointed distal, and was aligned closely with the anatomic Z-direction.

Three points were taken from the fibula load cell for each CT scan, and they included the posterior-most corner of the proximal face of the fibula load cell, the anterior-most corner of the proximal face of the fibula load cell, and the top screw hole on the proximal face of the fibula load cell. The positive X-direction of the fibula load cell coordinate system was formed by calculating the midpoint of the two proximal face corner points and subtracting that midpoint from the top screw hole of the proximal face of the fibula load cell. This vector was then normalized and plotted, to ensure it pointed from the curved surface of the fibula load cell towards the flat surface of the fibula load cell. The positive Y-direction was calculated by subtracting the posterior corner of the proximal face of the fibula load cell (point 1 in Figure 2, bottom) from the anterior corner of the fibula load cell (point 2 in Figure 2, bottom), and then normalizing this vector. This vector was only positive for right specimens, and needed to multiplied by negative one for left specimens in order to ensure the load cell coordinate system was accurate to the measured values. The positive Z-direction was calculated for the fibula load cell coordinate system by taking the cross product of the normalized positive X-axis vector and the positive Y-axis value. As in the development of previous coordinate systems, all positive axes were plotted, to ensure a right-handed coordinate system with the positive fibula load cell Z-axis aligned closely with the positive anatomic Z-axis.

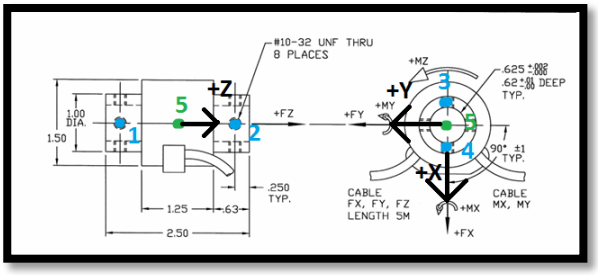

1	Proximal side screw hole on tibia LC
2	Distal side screw hole on tibia LC
3	Posterior proximal screw hole on tibia LC
4	Anterior proximal screw hole on tibia LC
5	Origin, calculated at middle of tibia LC

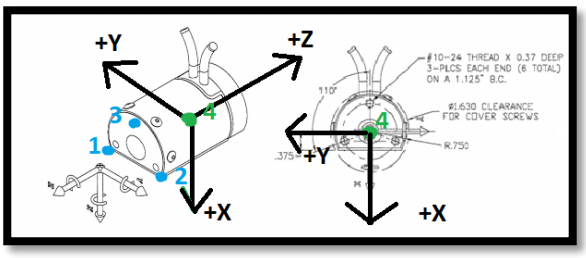

1	Posterior corner of proximal face of fibula LC (pictured for right foot)
2	Anterior corner of proximal face of fibula LC (pictured for right foot)
3	Top screw hole of proximal face of fibula LC
4	Origin, calculated at middle of fibula LC

Figure 3. Diagrams of tibia (top) and fibula (bottom) internal load cells and descriptions of the points taken to form the tibia and fibula load cell coordinate systems.

Transformation of Load Cell Data to be aligned with Anatomic Coordinate System

Three rotation matrices (including rotation and translation data) were formed from the creation of the anatomic coordinate system, the tibia load cell coordinate system and the fibula load cell coordinate system. Because these coordinate systems were formed by taking CT point in the CT coordinate system, it was possible to find the relationship between the anatomic coordinate system and the load cell coordinate system using the following multiplication of rotation matrices.

$$\begin{bmatrix} Tibia\ Load\ Cell\ in \\ Anatomic\ Coordinate\ system \end{bmatrix} = \begin{bmatrix} Tibia\ Load\ Cell\ in \\ CT\ Coordiante\ System \end{bmatrix} \begin{bmatrix} Anatomic\ in \\ CT\ Coordinate\ System \end{bmatrix}^T$$

$$\begin{bmatrix} Fibula\ Load\ Cell\ in \\ Anatomic\ Coordinate\ system \end{bmatrix} = \begin{bmatrix} Fibula\ Load\ Cell\ in \\ CT\ Coordiante\ System \end{bmatrix} \begin{bmatrix} Anatomic\ in \\ CT\ Coordinate\ System \end{bmatrix}^T$$

Then, the forces were transformed to the anatomic coordinate system using the above tibia load cell in the anatomic coordinate system and fibula load cell in anatomic coordinate system rotation matrices by the following matrix equations.

$$\begin{bmatrix} Tibia\ Fx\ in\ Anatomic\ CS \\ Tibia\ Fy\ in\ Anatomic\ CS \\ Tibia\ Fz\ in\ Anatomic\ CS \end{bmatrix} = \begin{bmatrix} Tibia\ Load\ Cell\ in \\ Anatomic\ CS \end{bmatrix} * \begin{bmatrix} Measured\ Tibia\ Fx \\ Measured\ Tibia\ Fy \\ Measured\ Tibia\ Fz \end{bmatrix}$$

$$\begin{bmatrix} Fibula\ Fx\ in\ Anatomic\ CS \\ Fibula\ Fy\ in\ Anatomic\ CS \\ Fibula\ Fz\ in\ Anatomic\ CS \end{bmatrix} = \begin{bmatrix} Fibula\ Load\ Cell\ in \\ Anatomic\ CS \end{bmatrix} * \begin{bmatrix} Measured\ Fibula\ Fx \\ Measured\ Fibula\ Fy \\ Measured\ Fibula\ Fz \end{bmatrix}$$

Footplate Load Cell Mass Compensation and Coordinate System

Inertial effects of the impactor assembly were taken into account by mass compensation of the footplate load cell. This mass compensation factor was calculated by multiplying the mass of half of the footplate load cell and the footplate by the average of the two footplate accelerometer traces. This factor was then subtracted from the measured footplate load cell, as seen in the equations below.

$$comp_{mass} = \frac{1}{2}\left(mass_{LC} + mass_{footplate}\right) * \frac{1}{2}\left(accel_1 + accel_2\right)$$

$$Footplate\ Force_{MassComp} = FootplateForce - comp_{mass}$$

Time-history data plots and corridors of initial footplate axial load data and mass compensated footplate axial force data are reported in the Results section.

Data Inclusion Analysis

ISO Analysis

ISO scores were calculated using the ISO objective rating metric for non-ambiguous signals (2013) to compare the shod and barefoot traces, in order to determine if there was a systematic difference in specimen kinematic or kinetic response as a result of the presence or absence of a show. This metric is only validated for time-history curves, and requires all curves to be the same length. Therefore, for this test series, ISO scores were only calculated for the time-histories of combined tibia and fibula axial load, tibia axial load, fibula axial load, knee axial load, mass compensated footplate axial load, and the footplate displacement. These scores were calculated for all tests, including Tests 3 and 4, which were performed in 2013 under a different NHTSA contract. The ISO score yields a result between 0 and 1 (1 being a perfect fit). The total ISO rating results from the weighting of the four sub-metric ratings: corridor (weighted 0.4 of ISO score), phase (weighted 0.2 of ISO score), magnitude (weighted 0.2 of ISO score), and slope (weighted 0.2 of ISO score). The corridor metric calculates the deviation between two signals by means of corridor fitting. The phase score is used to measure the phase lag between the two time histories, which contains a maximum allowable percentage of time shift ε, with ε=0.2, with the maximum allowable time shift limits being ε*(t(end)-t(start)). The magnitude score is defined as the difference in amplitude of the two time histories at the same time step. A cost function with the input of the difference in amplitude in the two traces is used to calculate the magnitude score. The slope error is calculated between the two compared curves, by calculating the discrepancy in slope at each point, with a maximum allowed error. ISO defines the scores total ISO scores as the following.

1 > ISO > 0.94	Excellent	0.8 > ISO > 0.5	Fair
0.94> ISO > 0.8	Good	ISO < 0.5	Poor

Results for Shod Versus Barefoot Data Traces

Total Cross Sectional Combined Tibial and Fibular Load Versus Time

Table 2. Calculated ISO scores for the shod versus barefoot PMHS total tibia and fibula axial forces versus time.

Test	ISO	Corridor	Phase	Magnitude	Slope
4 v 3*	.83	.90	.88	.85	.62
16 v 15	.85	.91	.92	.77	.73
17 v 18	.85	.90	.96	.84	.63
19 v 20	.83	.92	.96	.85	.51
22 v 21	.87	.96	.96	.84	.62

24 v 23	.89	.96	.92	.84	.76
26 v 25	.77	.83	.92	.74	.54
Shod v Barefoot	.84	.91	.93	.82	.63

Tibia Axial Load Versus Time

Table 3. Calculated ISO scores for the shod versus barefoot PMHS tibia axial forces plotted against time.

Test	ISO	Corridor	Phase	Magnitude	Slope
4 v 3	.81	.86	.88	.84	.59
16 v 15	.82	.92	.92	.64	.72
17 v 18	.83	.88	.92	.87	.62
19 v 20	.84	.93	.96	.82	.57
22 v 21	.81	.93	.96	.71	.53
24 v 23	.89	.96	.96	.84	.72
26 v 25	.77	.84	.96	.72	.52
Shod v Barefoot	.83	.90	.94	.78	.61

Fibula Axial Load Versus Time

Table 4. Calculated ISO scores for the shod versus barefoot PMHS fibula axial forces plotted against time.

Test	ISO	Corridor	Phase	Magnitude	Slope
4 vs 3	.80	.87	.96	.74	.57
16 v 15	.80	.86	.84	.82	.62
17 v 18	.72	.83	.80	.71	.44
19 v 20	.76	.85	.84	.71	.53
22 v 21	.77	.82	.84	.76	.62
24 v 23	.75	.79	.92	.54	.71
26 v 25	.75	.83	.88	.70	.53
Shod v Barefoot	.70	.84	.87	.71	.57

Knee Axial Load Versus Time

Table 5. Calculated ISO scores for the shod versus barefoot PMHS knee axial forces plotted against time.

Test	ISO	Corridor	Phase	Magnitude	Slope
4 v 3	.80	.87	.96	.74	.57
16 v 15	.84	.91	.92	.71	.78
17 v 18	.83	.89	.96	.86	.57
19 v 20	.81	.91	.92	.82	.52
22 v 21	.85	.95	.96	.80	.58
24 v 23	.90	.96	.92	.88	.77
26 v 25	.76	.83	.92	.67	.56
Shod v Barefoot	.83	.90	.94	.78	.62

Footplate Axial Load Versus Time

Table 6. Calculated ISO scores for the shod versus barefoot PMHS mass compensated footplate axial forces plotted against time.

Test	ISO	Corridor	Phase	Magnitude	Slope
4 v 3	.81	.86	.88	.84	.59
16 v 15	.82	.92	.92	.64	.72
17 v 18	.83	.88	.92	.87	.62
19 v 20	.84	.93	.96	.82	.57
22 v 21	.81	.93	.96	.71	.53
24 v 23	.89	.96	.96	.84	.72
26 v 25	.77	.84	.96	.72	.52
Shod v Barefoot	.83	.90	.94	.78	.61

Footplate Displacement Versus Time

Table 7. Calculated ISO scores for the shod versus barefoot PMHS footplate displacements plotted against time.

Test	ISO	Corridor	Phase	Magnitude	Slope
4 v 3	.82	.77	.86	.91	.81
16 v 15	.73	.62	.84	.78	.78
17 v 18	.48	.54	.72	0	.57
19 v 20	.86	.90	.92	.91	.68
22 v 21	.96	.99	.96	.97	.89
24 v 23	.90	.89	.92	.90	.88
26 v 25	.60	.70	.64	.30	.67
Shod v Barefoot	.75	.76	.85	.66	.73

The ISO analysis demonstrated limited systematic difference between the shod and barefoot datasets, with the differences tending to be concentrated in the magnitude and slope ratings. Because of the limited systematic differences observed, it was decided to continue to explore the option of combining the shod and the barefoot datasets into the corridors by creating corridors from the combined dataset, as well as the shod and barefoot datasets individually.

Test 3 and Test 15 Exclusion from Corridor Development

An initial examination of the dataset showed that Tests 3 and 15, (the barefoot test from 2013, and the initial test from the most recent test series), had a substantial effect on the shape of some portions of the corridor, as seen in Figure 3, below. Both these tests caused the corridors increased with width of the corridors, predominantly by driving the shape and location of the corridor upper bounds.

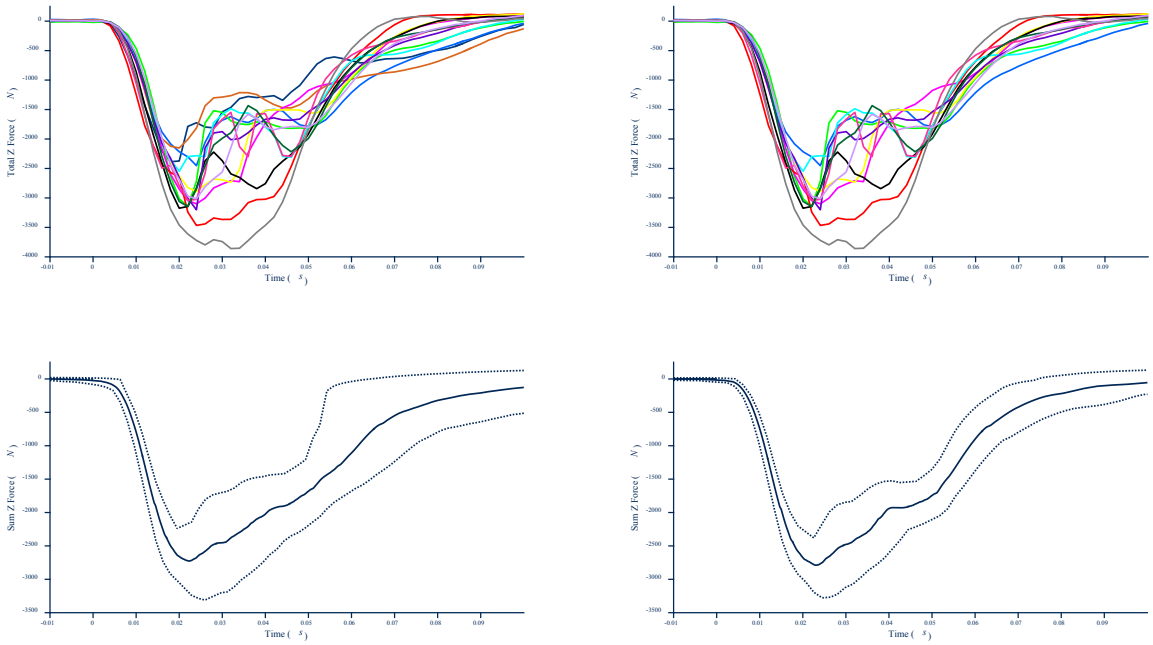

Figure 4. Representative example of how Tests 3 and 15 skew corridor development. All data traces, including Tests 3 and 15, plotted in navy blue and orange are shown on top left. Top right figure shows all data traces for the combined tibia and fibula axial load without Tests 3 and 15. Bottom left depicts the corridor for combined tibia and fibula axial force versus time resulting from including Tests 3 through 26. Bottom right shows the resulting corridor from the above data traces when Tests 3 and 15 are removed and only Test 4, and Tests 16 through 26 are used to form the corridors.

Because of the strong effect of Test 15 on the shape of the corridors, the kinematics and response of these tests compared to all of the other tests were carefully examined. High speed video analysis showed both Tests 3 and 15 demonstrated different kinematics (the tibia and fibula arched upward during the test) and Test 15 showed a different injury pattern (the only specimen to obtain a

fracture in the potting cups). These differences in kinematics are likely due to a difference in positioning, with the tibia and fibula being angled with the heel higher than the knee, rather than the leg being positioned parallel to the floor and the direction of loading. This difference in position resulted in a slightly different angle of loading, and resulting kinematic and force trace differences in these two tests, and thus they were excluded in the formation of corridors. This resulted in a total of 12 tests used for combined corridor formation, 7 tests for shod corridor development, and 5 tests for barefoot corridor development.

Corridor Development Methodology

Test Data Corridor Development

Corridors were constructed using a combined arc length parameterization of the data, followed by a method described by Ash et al. (2012), in which a characteristic average curve is calculated, and ellipses representing the standard deviations are calculated to form the corridor bounds (Donlon, Joodaki, Toczyski, Lessley, & Forman, 2016). Using the assumption that the responses are geometrically similar, each response is parameterized by the distance along the curve. The arc length parameter is normalized by the distance along the curve between two characteristic points (start of response, peak of response). In the dataset below, all traces were parameterized using the start of the response and the minimum peak of the response, with the exception of the axial footplate load, which was parameterized using the start of the response and the maximum peak of the response. This parameterization allows the two dimensions of the response to be described as a function of normalized arc-length. Using this arc length parametrized data, the method of corridor formation creates an average curve that captures the shape and average phase of the underlying data, and then ellipses are calculated at each point on the average curve that represent ±1 standard deviation in both the independent (phase) and dependent (response), variables at each point in time. The ellipses are swept along the length of the curve, forming the basis for a ±1 standard deviation corridor.

Justification of Using 500 Hz Data

Data sampled at 10,000 Hz and 500 Hz was analyzed for use in corridor development. Figure 4 shows the similarity between the 10,000 Hz sampled data and the 500 Hz sampled data when an individual data trace was plotted against time. This was a consistent trend for all data traces when they were down sampled. An additional analysis was performed to generate corridors with the same traces using data sampled either at 500 Hz and data sampled at 10,000 Hz. The corridors formed with the two different sampling rates resulted in corridor and average traces within 2 percent error of one another.

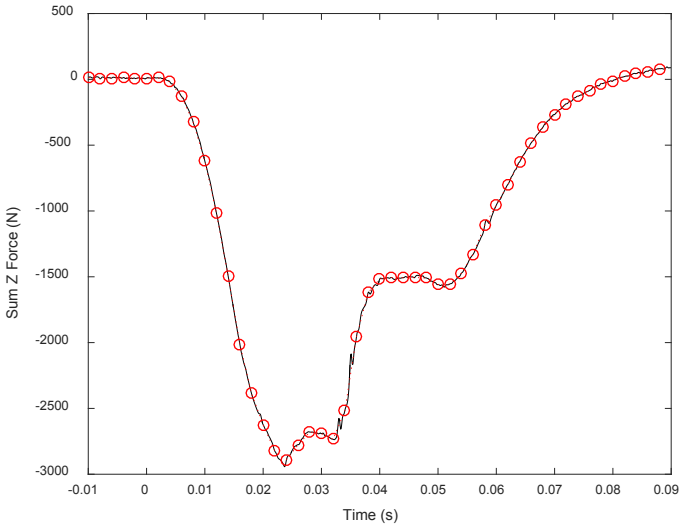

Figure 5. The figure on the left depicts the total sum Z force of one data trace plotted at 500 Hz (red dots) and 10,000 Hz (black line). Down sampling the data has very little effect on the features of the individual data traces, and even less on the mean trace reported in the corridors.

500 Hz data was chosen to be used for the formation of all the corridors for two reasons: the lower sampling rate still captured all of the features of the force traces and corridors, and computational time for the corridor creation was decreased for data sampled at 500 Hz. Given the number of corridors to be created for the axial loading test series, and the fact that down sampling the data did not result in reduced corridor accuracy, the 500 Hz sampled data was used to form all of the corridors reported in this study.

Scaling Methodology

Equal-Stress Equal-Velocity Scaling Methodology

While this study attempted to use PMHS close to the anthropometry (height and weight) of the 5th percentile female, all the tested PMHS were taller and/or heavier than the target anthropometry. This makes sense, as by definition, the 5th percentile female almost does not exist in the population. Previous studies of male PMHS data have shown that measured force and kinematic response within the lower extremity for the same impact varies for different gross anthropometries, like total weight and total height, and often with more local anthropometries, like leg length or foot mass (Funk et al., 2002; Kuppa, Wang, Haffner, & Eppinger, 2001; Kerrigan et al., 2004). In the past, both length and mass based metrics have been used to generate scaling factors to predict the internal force response for PMHS of different anthropometries in order to predict the response of a target anthopometry; this is sometimes called normalizing the response (Untario et al., 2007;Yoganandan, Arun, & Pintar, 2014). Given that all the small female PMHS tested in the

axial load condition were larger than the target anthropometry, scaling was applied in attempt to predict the axial loading response of the lower extremity for the 5th percentile female occupant.

Equal-stress equal-velocity scaling methodology developed by Eppinger was used for all of the scaled PMHS data in this report (1976). This scaling technique assumes linear relationships between length, mass and time, described by the following equations:

$$L_{ATD} = \lambda_l * L_{PMHS}$$

$$M_{ATD} = \lambda_m * M_{PMHS}$$

$$T_{ATD} = \lambda_t * T_{PMHS}$$

This scaling method also assumes equal density and modulus of elasticity between the two scaled quantities. Only forces, time, and displacement data were scaled in this dataset, so only a scaling factor determine from length was needed for this dataset. The scaling equations used for this test set were:

$$F_{ATD} = {\lambda_l}^2 * F_{PMHS}$$

$$t_{ATD} = \lambda_l * t_{PMHS}$$

$$d_{ATD} = \lambda_l * d_{PMHS}$$

$$\text{With:} \quad \lambda_l = \frac{Characteristic\ Length_{ATD}}{Characteristic\ Length_{PMHS}}$$

For this test series, two different characteristic length scaling factors were calculated, one based on the total height, and another based on the leg length from the joint center of the ankle to the joint center of the knee for the 5th percentile ATD and the tested PMHS.

Total Height Versus Leg Length scaling

Table 7 shows a test matrix of the conditions for each test, as well as the total height and leg length for each specimen. Tests 3 and 4 were performed in 2013, while the remaining tests were performed for this solicitation. The total height metric was reported by vendors from which the tested PMHS were obtained. Most PMHS used in this test series were obtained as leg-only components, so total height of each specimen could not be directly measured. The goal of the leg length metric from the PMHS was to correspond to the distance from the center of the ankle joint to the center of the knee joint from the THOR 5th female ATD (342.1 mm). The center of the ankle joint was measured as the midpoint of the lateral and medial malleoli measured from CT scans of each specimen. This midpoint between the two malleoli has been demonstrated to be a reasonable approximation of the center of the ankle joint (Lundberg, Svensson, Nemeth, & Selvik, 1989). Literature also shows that the center of the average male knee joint is close to 44.4 mm radial distance from the top surface of the tibial plateau (Hollister, Jatana, Singh, Sullivan, &

Lupichuk, 1993). Scaling this radius (using equal-stress, equal-velocity scaling with the total heights of the 50th percentile male and the 5th percentile female), this radial distance becomes 38.44 mm from the tibial plateau for the 5th percentile female. To approximate the leg length corresponding to ankle center to knee center, the distance between the midpoint of the lateral and medial malleoli, and the midpoint of the most lateral and most medial points of the tibial plateau was calculated from each CT scan, and then 38.44 mm was added to each of these measurements. Leg length and total height were analyzed to determine which length scaling factor would be more accurate for corridor development.

Table 8. Test conditions and scaling measurements for each PMHS. A * before the test number indicates that the test was not included in corridor development (Tests 3 and 15).

Test #	Specimen	Condition	Height (cm)	Tibia Length (mm)	Leg Length (mm)
-	F-05 ATD	-	152	-	342.1
*Test 15	820 R	Barefoot	160	369.14	407.54
Test 16	820 L	Shod	160	372.00	410.40
Test 17	822 L	Shod	160	373.12	411.52
Test 18	822 R	Barefoot	160	371.18	409.58
Test 19	840 R	Shod	160	339.40	377.80
Test 20	840 L	Barefoot	160	338.21	376.61
Test 21	841 L	Barefoot	146.4	320.36	358.76
Test 22	841 R	Shod	146.4	328.98	367.38
Test 23	844 R	Barefoot	160	335.25	373.65
Test 24	844 L	Shod	160	341.24	379.64
Test 25	845 L	Barefoot	162.6	366.67	405.07
Test 26	845 R	Shod	162.6	364.60	403.00
*Test 3	668 R	Barefoot	157.48	338.01	376.41
Test 4	668 L	Shod	157.48	332.88	371.28

As a result of forming initial corridors with both total height scaling (seen in Figure 4, below), and leg length scaling, the leg length scaling, was chosen as the characteristic scaling length for all of the scaled corridor formation. Leg length scaling from the initial formation yielded narrower corridors as compared to total height scaled data. Additionally, since most PMHS used in this study were obtained as leg-only components, direct measure of the leg length is likely more reliable, precise, and accurate than the total body heights reported by the suppliers.

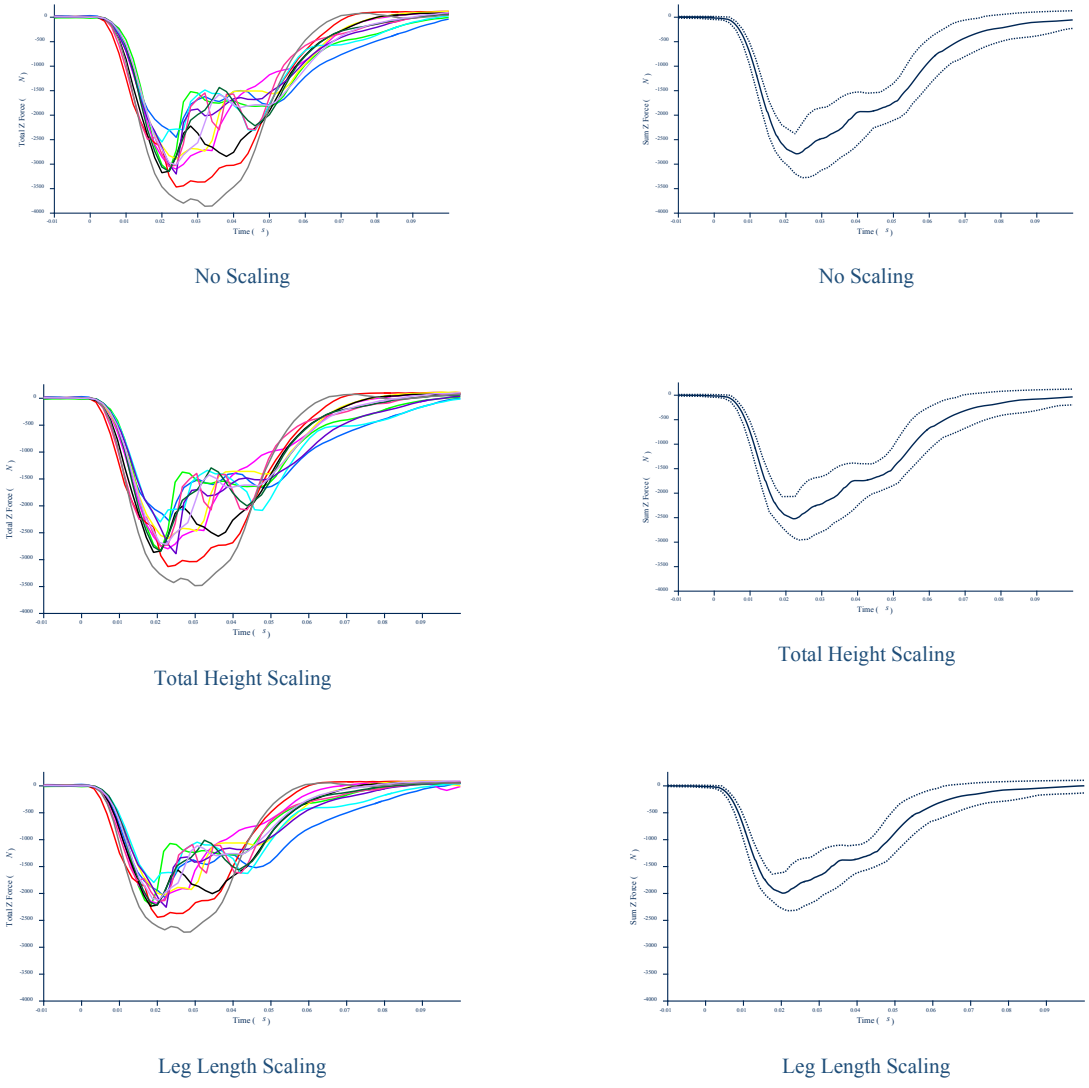

Figure 6. Unscaled and scaled data and the resulting corridors for combined tibia and fibula axial force versus time are shown above. All plots on the left hand side show the individual data traces that contribute to the formation of a corridor, and all plots on the right are the resulting corridors. Original data is plotted on the top. Data scaled by total specimen height are shown in the middle two plots. Data scaled by leg length is shown on the bottom two plots.

Corridors are plotted in 12 sections: combined dataset versus time corridors (Figures 7-12), shod datasets versus time corridors (Figures 13-18), barefoot dataset versus time corridors (Figures 19-24), combined dataset versus footplate displacement corridors (Figures 25-29), shod dataset versus footplate displacement corridors (Figures 30-34), barefoot datasets versus footplate displacement corridors (Figures 35-39), and leg length scaled data corridors for each of the previously mentioned categories (Figures 40-71). The data for each individual test is plotted in all of the below figures in the colors shown in Table 8.

Table 9. Color scheme for each individual test plotted in Figures 5-71, below.

Combined Shod and Barefoot Corridors		Shod Corridors		Barefoot Corridors	
Test 4		Test 4		Test 18	
Test 16		Test 16		Test 20	
Test 17		Test 17		Test 21	
Test 18		Test 19		Test 23	
Test 19		Test 22		Test 25	
Test 20		Test 24		-	
Test 21		Test 26		-	
Test 22		-		-	
Test 23		-		-	
Test 24		-		-	
Test 25		-		-	
Test 26					

Results: Combined Shod and Barefoot Data Corridors Versus Time

Tibia Axial Load Versus Time

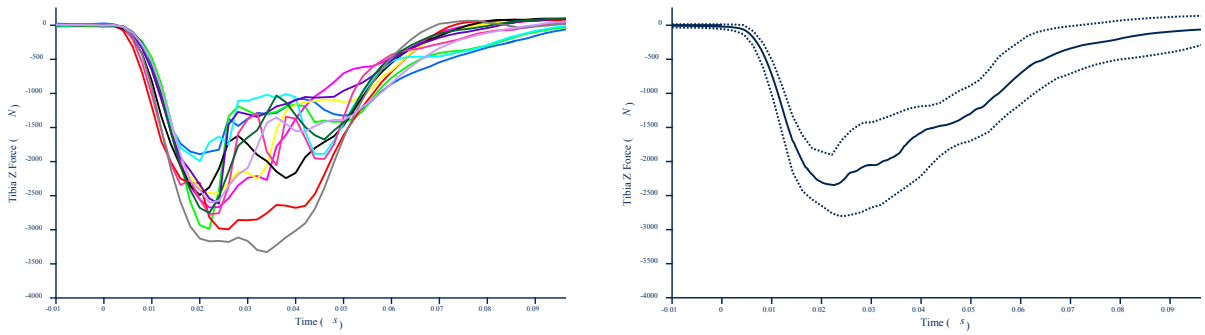

Figure 7. Data traces for all 12 tests for the axial force measured in the tibia versus time (left) and the resulting corridor from those data traces (right).

Fibula Axial Load Versus Time

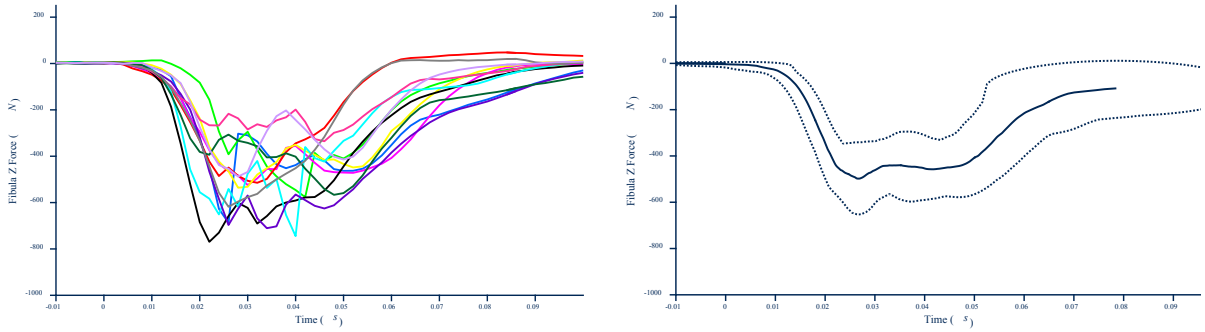

Figure 8. Data traces for all 12 tests for the axial force measured in the fibula versus time (left) and the resulting corridor from those data traces (right).

Total Cross Sectional Combined Tibial and Fibular Load Versus Time

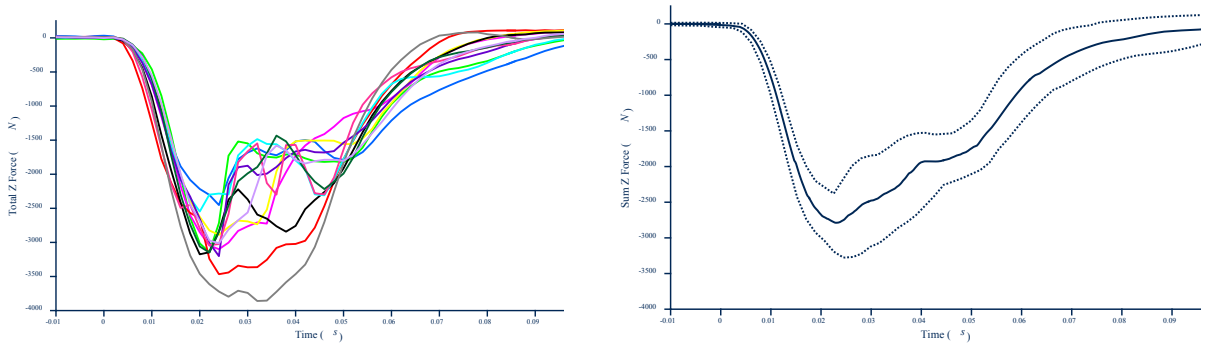

Figure 9. Data traces for all 12 tests for the combined axial force measured in the tibia and fibula versus time (left) and the resulting corridor from those data traces (right).

Knee Axial Load Versus Time

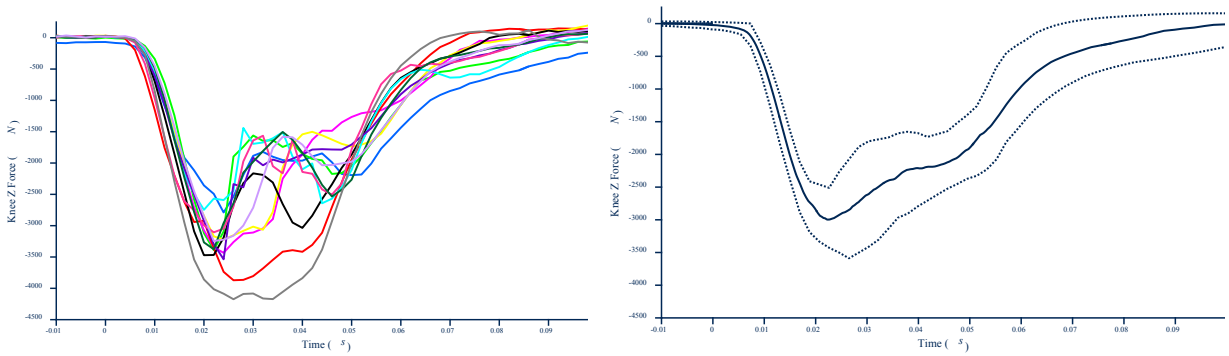

Figure 10. Data traces for all 12 tests for the axial force measured from the knee load cell versus time (left) and the resulting corridor from those data traces (right).

Footplate Displacement Versus Time

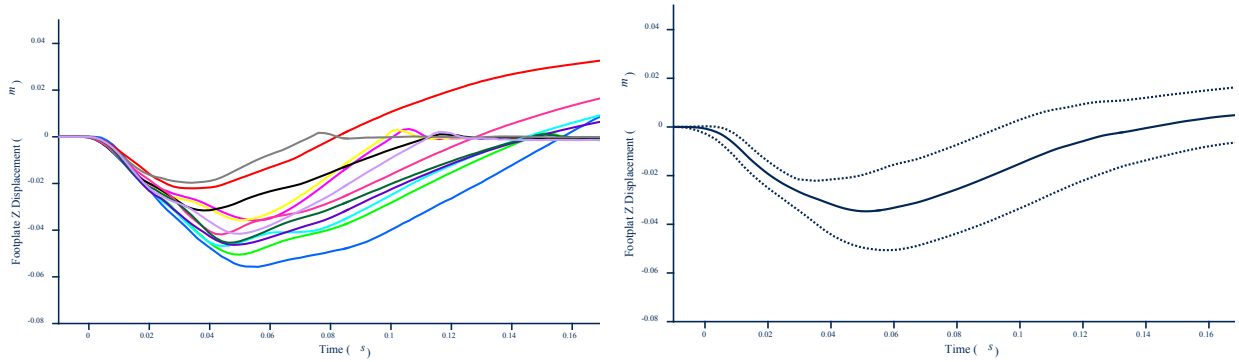

Figure 11. Data traces for all 12 tests for the footplate displacement versus time (left) and the resulting corridor from those data traces (right).

Footplate Axial Load (mass compensated) Versus Time

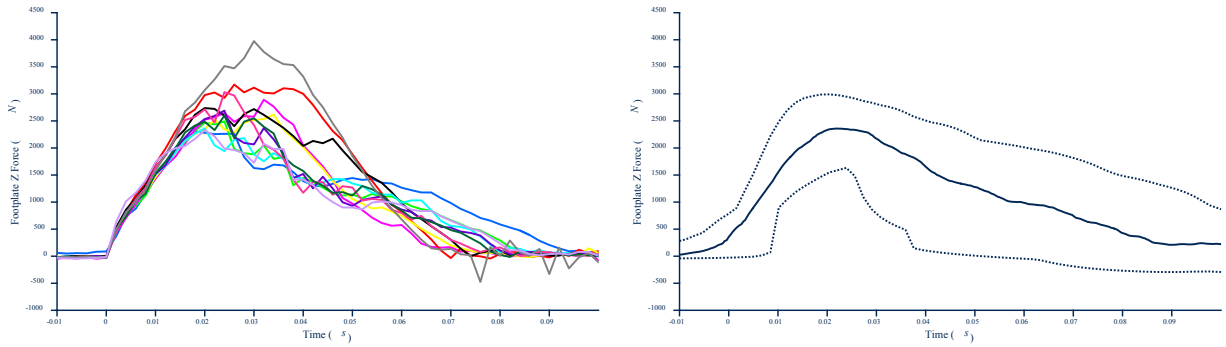

Figure 12. Data traces for all 12 tests for the axial force mass compensated footplate load cell versus time (left) and the resulting corridor from those data traces (right).

Results: Shod Corridors Versus Time

Tibia Axial Load Versus Time

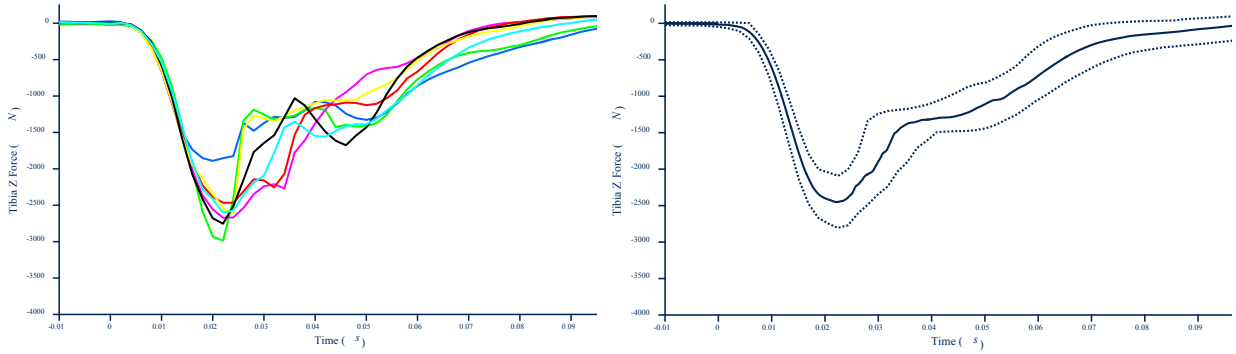

Figure 13. Data traces for the 7 shod tests for the axial force measured in the tibia versus time (left) and the resulting corridor from those data traces (right).

Fibula Axial Load Versus Time

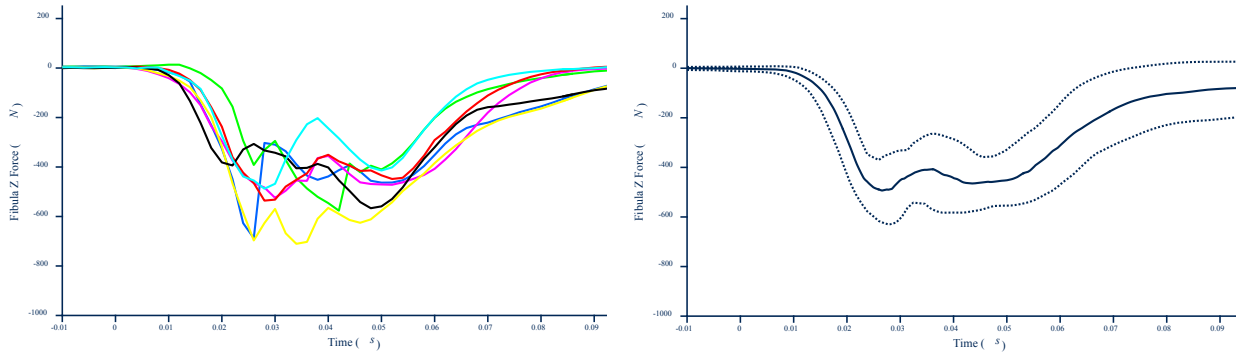

Figure 14. Data traces for the 7 shod tests for the axial force measured in the fibula versus time (left) and the resulting corridor from those data traces (right).

Total Cross Sectional Combined Tibial and Fibular Load Versus Time

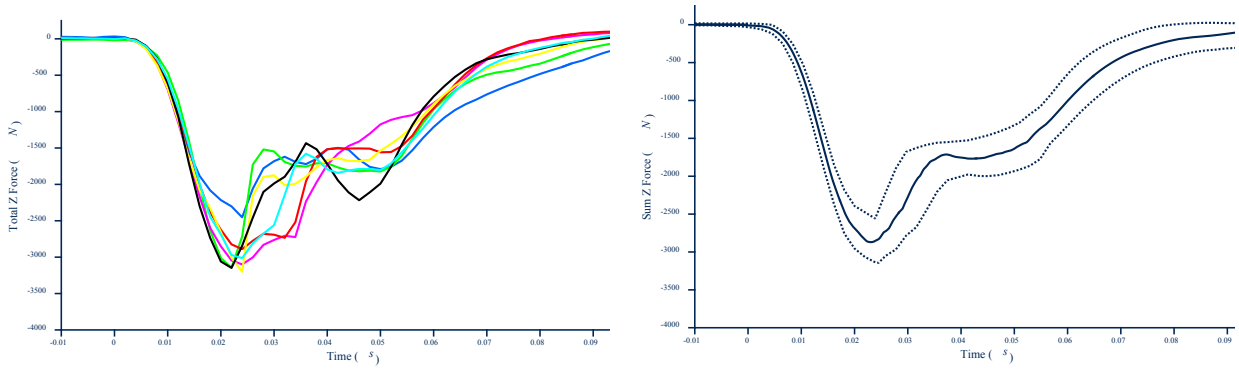

Figure 15. Data traces for the 7 shod tests for the axial force combined in the tibia and fibula versus time (left) and the resulting corridor from those data traces (right).

Knee Axial Load Versus Time

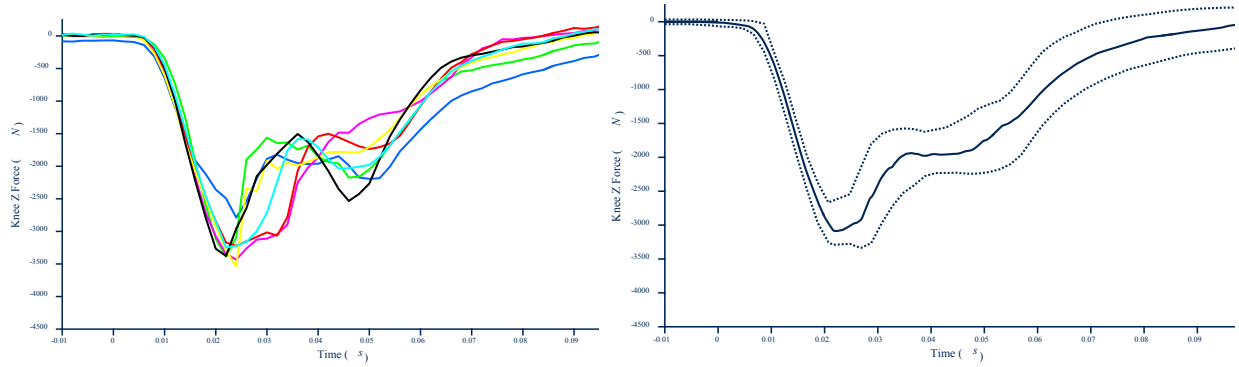

Figure 16. Data traces for the 7 shod tests for the axial force measured in the knee load cell versus time (left) and the resulting corridor from those data traces (right).

Footplate Displacement Versus Time

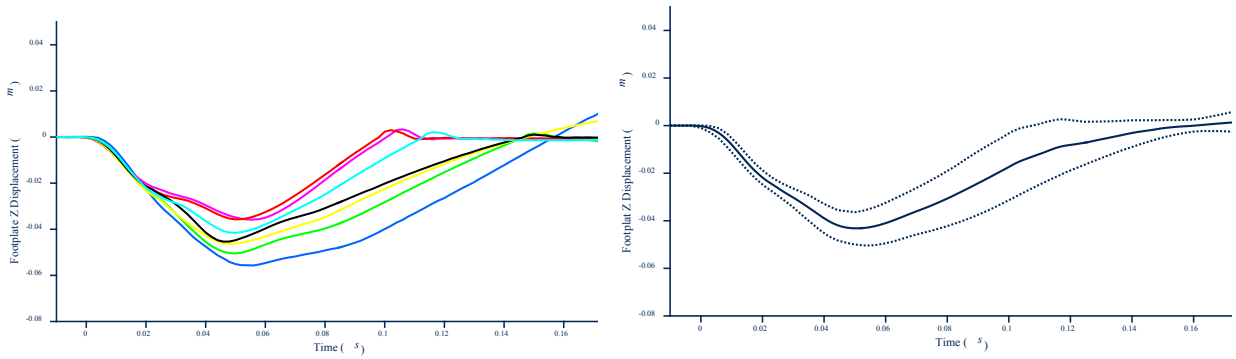

Figure 17. Data traces for the 7 shod tests for the footplate displacement versus time (left) and the resulting corridor from those data traces (right).

Footplate Axial Load (mass compensated) Versus Time

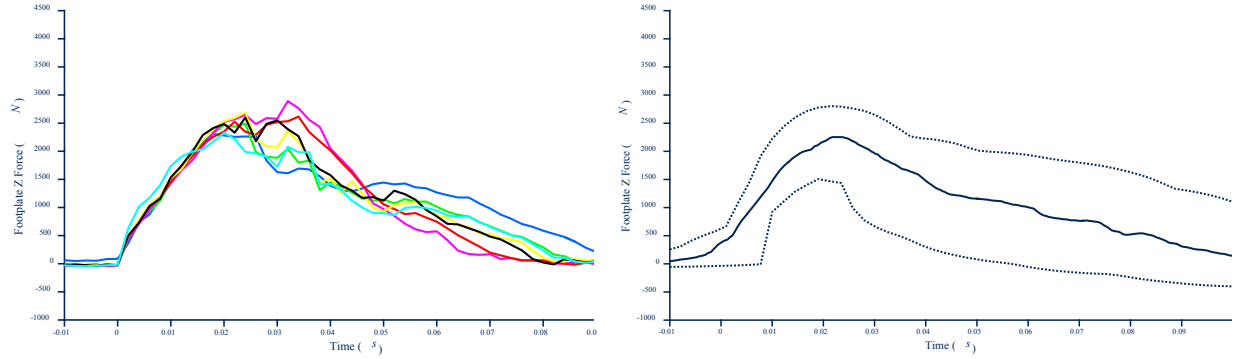

Figure 18. Data traces for the 7 shod tests for the axial force calculated for the mass compensated footplate load cell versus time (left) and the resulting corridor from those data traces (right).

Results: Barefoot Corridors Versus Time

Tibia Axial Load Versus Time

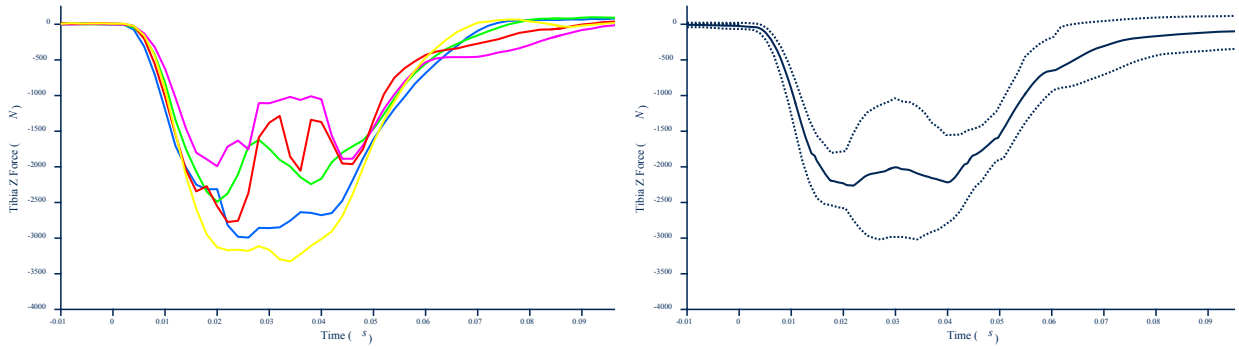

Figure 19. Data traces for the 5 barefoot tests for the axial force measured in the tibia versus time (left) and the resulting corridor from those data traces (right).

Fibula Axial Load Versus Time

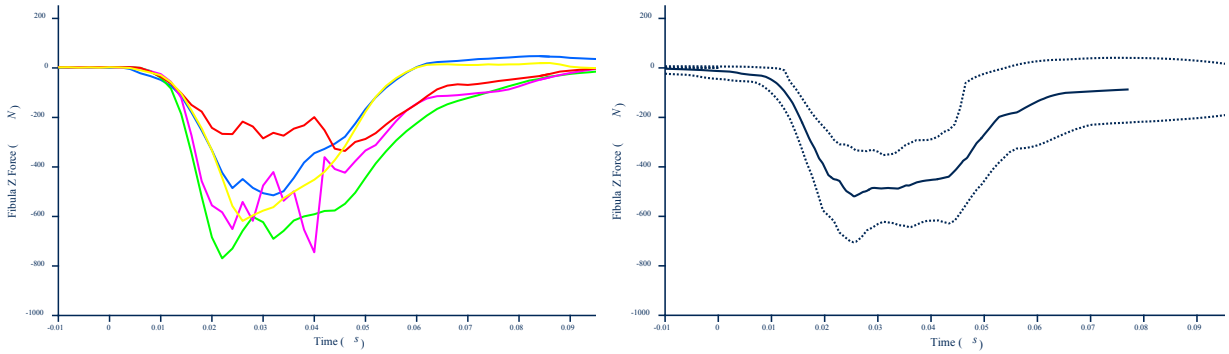

Figure 20. Data traces for the 5 barefoot tests for the axial force measured in the fibula versus time (left) and the resulting corridor from those data traces (right).

Total Cross Sectional Combined Tibial and Fibular Load Versus Time

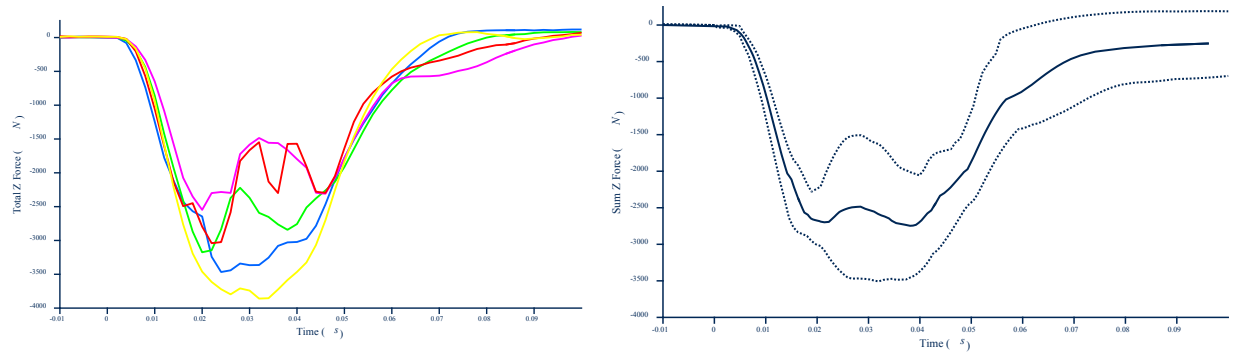

Figure 21. Data traces for the 5 barefoot tests for the axial force calculated in the combined tibia and fibula versus time (left) and the resulting corridor from those data traces (right).

Knee Axial Load Versus Time

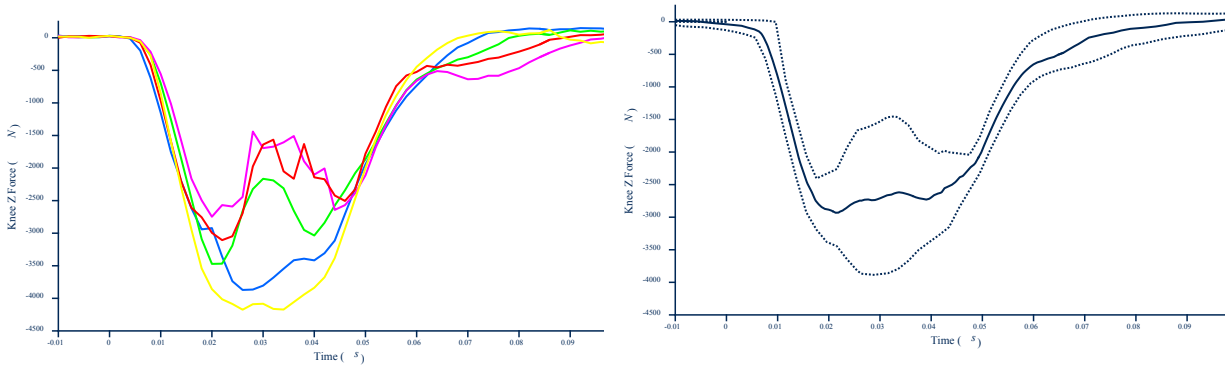

Figure 22. Data traces for the 5 barefoot tests for the axial force measured in the knee load cell versus time (left) and the resulting corridor from those data traces (right).

Footplate Displacement Versus Time

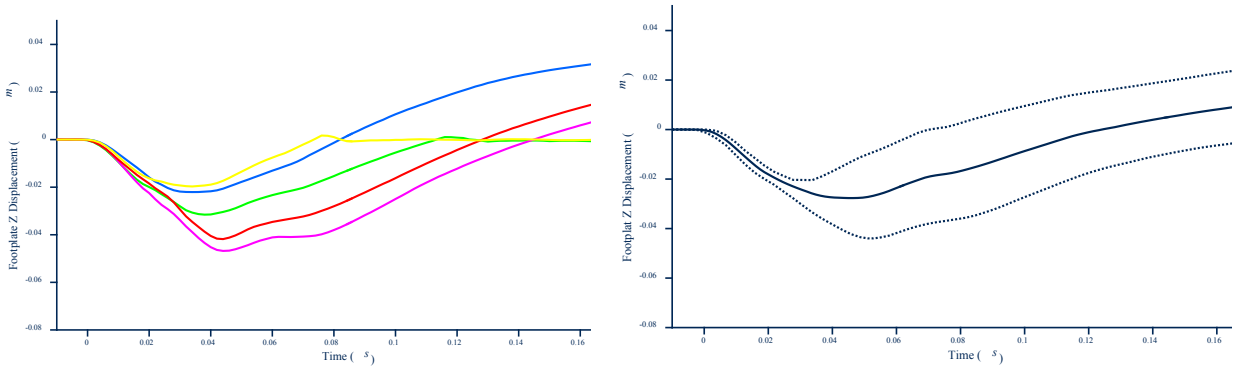

Figure 23. Data traces for the 5 barefoot tests for footplate displacement versus time (left) and the resulting corridor from those data traces (right).

Footplate Axial Load (mass compensated) Versus Time

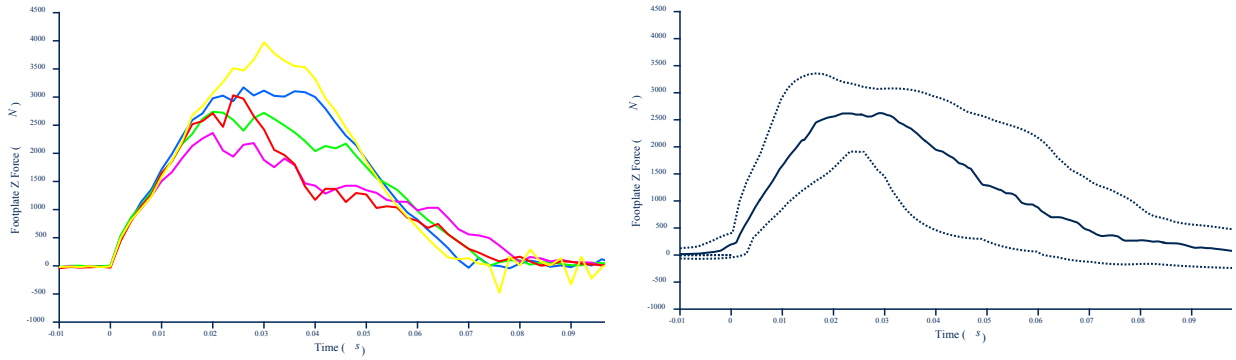

Figure 24. Data traces for the 5 barefoot tests for the axial force calculated for the mass compensated footplate load cell versus time (left) and the resulting corridor from those data traces (right).

Results: Combined Shod and Barefoot Data Corridors Versus Displacement

Tibia Axial Load Versus Footplate Displacement (all signals cropped at maximum displacement)

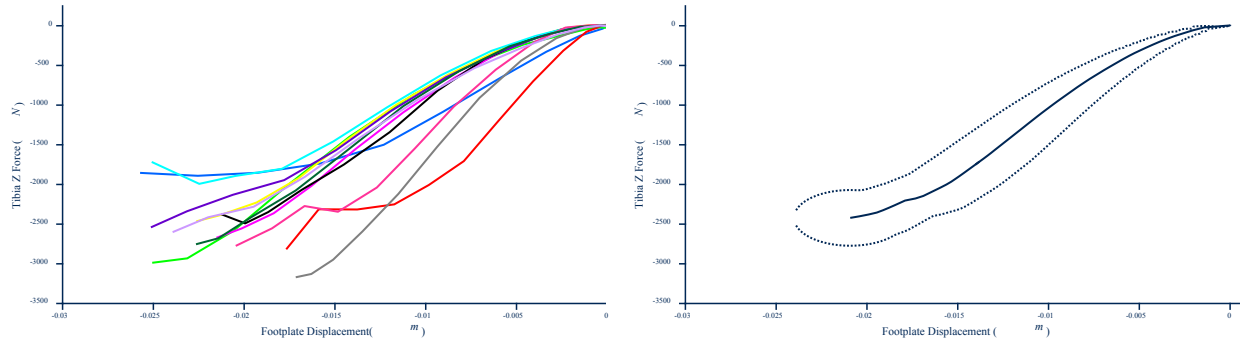

Figure 25. Data traces for all 12 tests for the axial force measured in the tibia versus footplate displacement (left) and the resulting corridor from those data traces (right).

Fibula Axial Load Versus Footplate Displacement

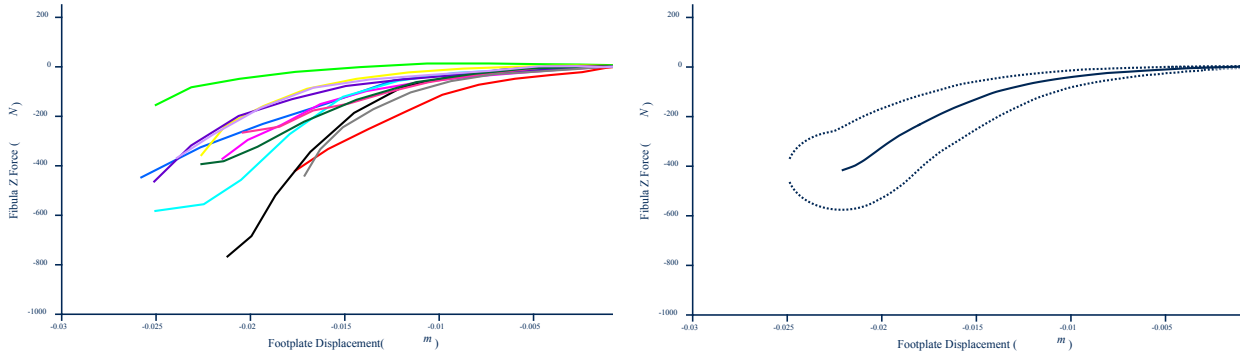

Figure 26. Data traces for all 12 tests for the axial force measured in the fibula versus footplate displacement (left) and the resulting corridor from those data traces (right).

Total Cross Sectional Combined Tibial and Fibular Load Versus Footplate Displacement

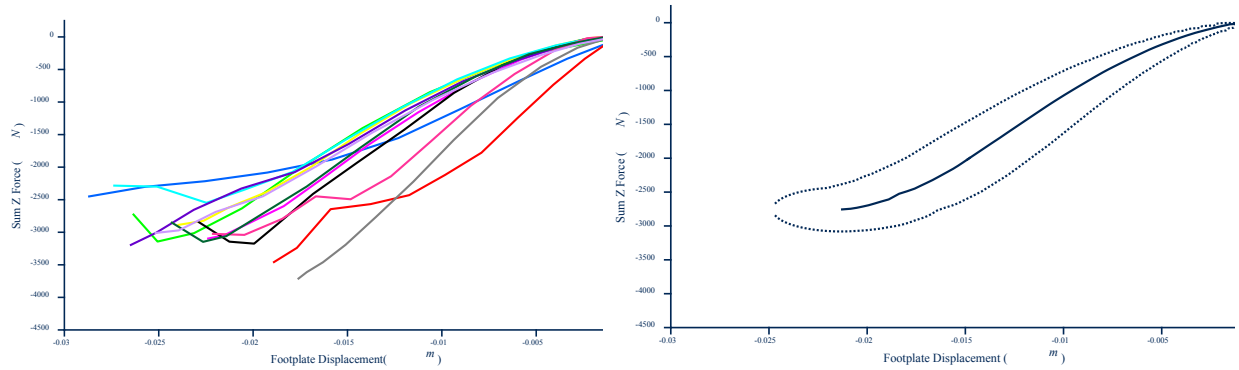

Figure 27. Data traces for all 12 tests for the axial force combined in the tibia and fibula versus footplate displacement (left) and the resulting corridor from those data traces (right).

Knee Axial Load Versus Footplate Displacement

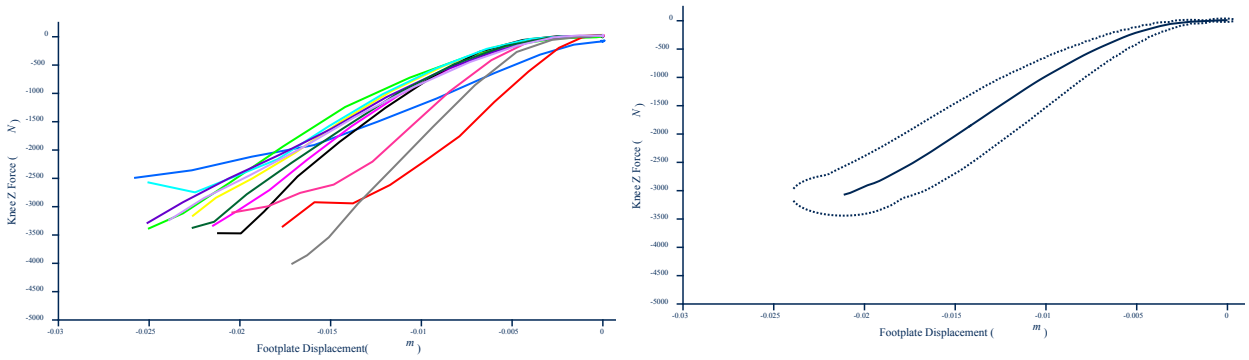

Figure 28. Data traces for all 12 tests for the axial force measured in the knee load cell versus footplate displacement (left) and the resulting corridor from those data traces (right).

Footplate Axial Load (mass compensated) Versus Footplate Displacement

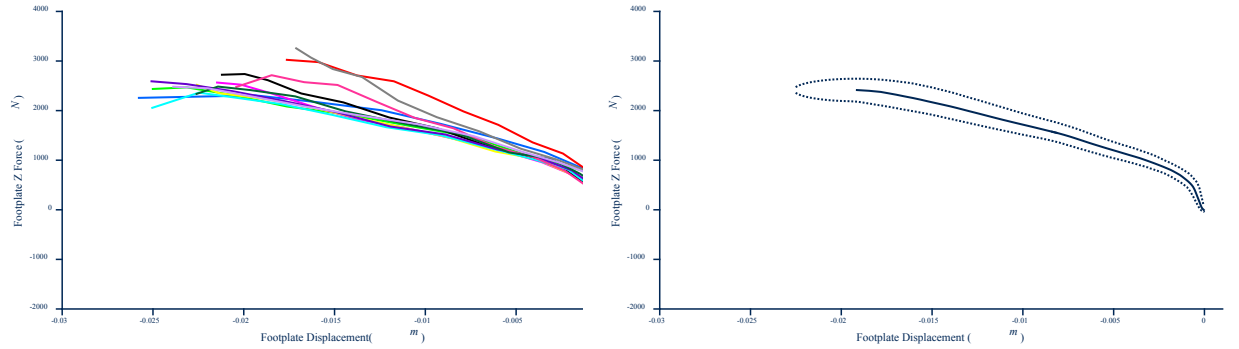

Figure 29. Data traces for all 12 tests for the axial force for the calculated mass compensated footplate load cell versus footplate displacement (left) and the resulting corridor from those data traces (right).

Results: Shod Data Corridors Versus Displacement

Tibia Axial Load Versus Footplate Displacement

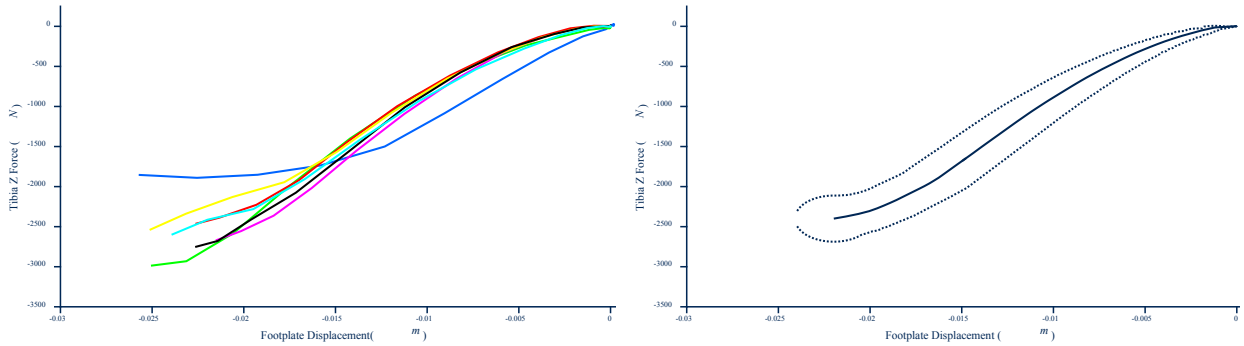

Figure 30. Data traces for the 7 shod tests for the axial force measured in the tibia versus footplate displacement (left) and the resulting corridor from those data traces (right).

Fibula Axial Load Versus Footplate Displacement

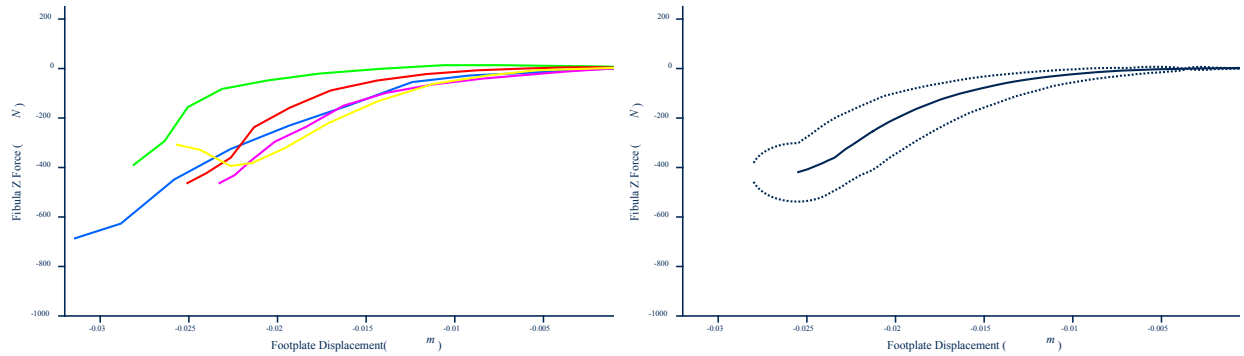

Figure 31. Data traces for the 7 shod tests for the axial force measured in the fibula versus footplate displacement (left) and the resulting corridor from those data traces (right).

Total Cross Sectional Combined Tibial and Fibular Load Versus Footplate Displacement

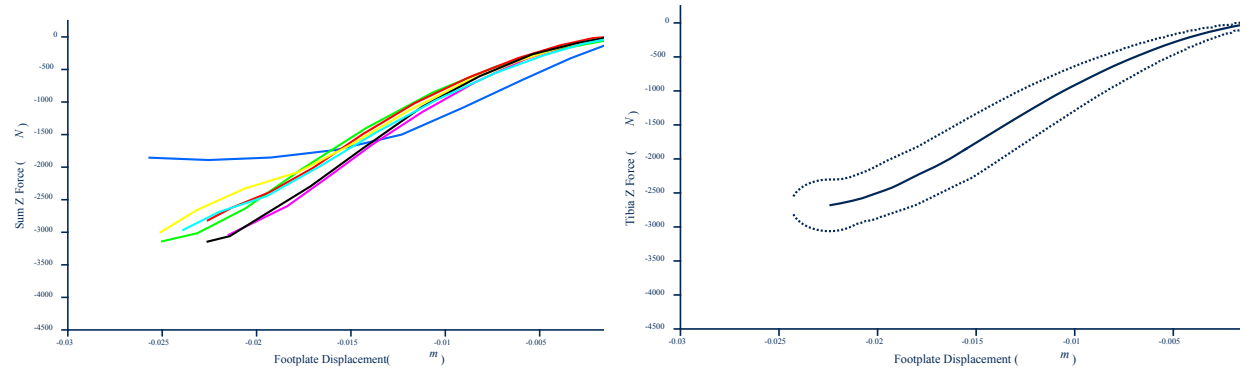

Figure 32. Data traces for the 7 shod tests for the axial force combined in the tibia and fibula versus footplate displacement (left) and the resulting corridor from those data traces (right).

Knee Axial Load Versus Footplate Displacement

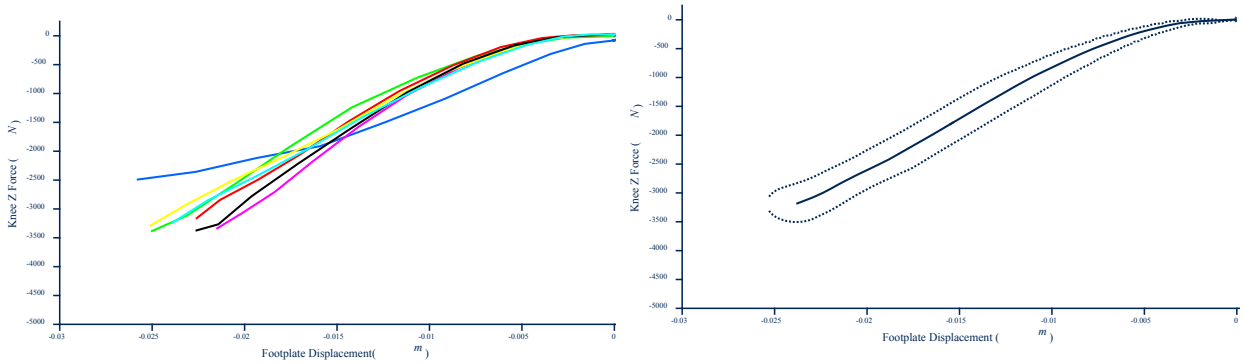

Figure 33. Data traces for the 7 shod tests for the axial force measured in the knee load cell versus footplate displacement (left) and the resulting corridor from those data traces (right).

Footplate Axial Load (mass compensated) Versus Footplate Displacement

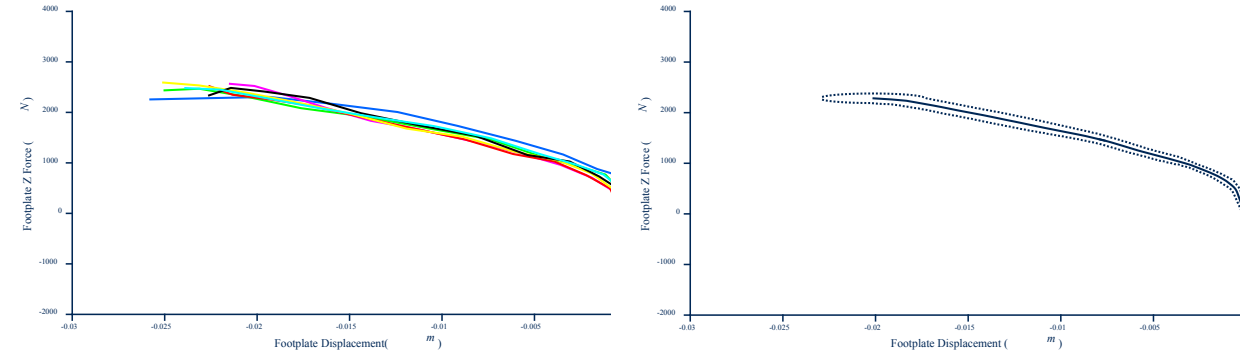

Figure 34. Data traces for the 7 shod tests for the axial force calculated in the mass compensated load cell versus footplate displacement (left) and the resulting corridor from those data traces (right).

Results: Barefoot Data Corridors Versus Displacement

Tibia Axial Load Versus Footplate Displacement

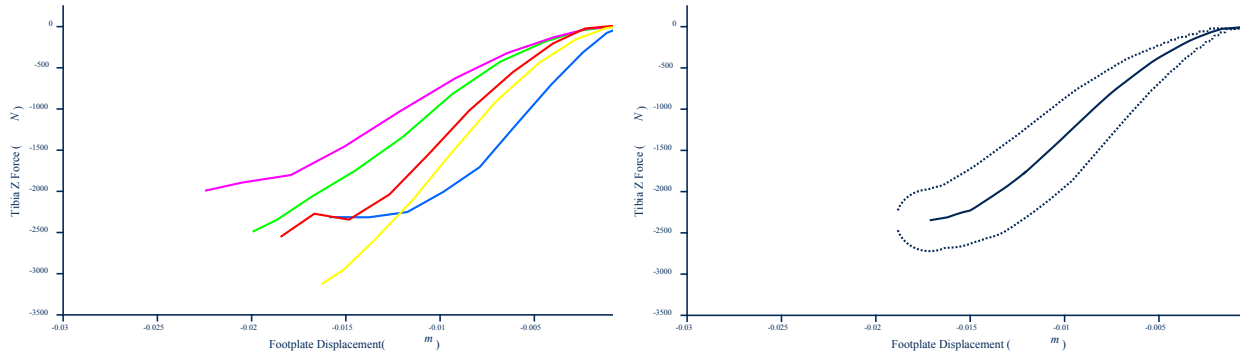

Figure 35. Data traces for the 5 barefoot tests for the axial force measured in the tibia versus footplate displacement (left) and the resulting corridor from those data traces (right).

Fibula Axial Load Versus Footplate Displacement

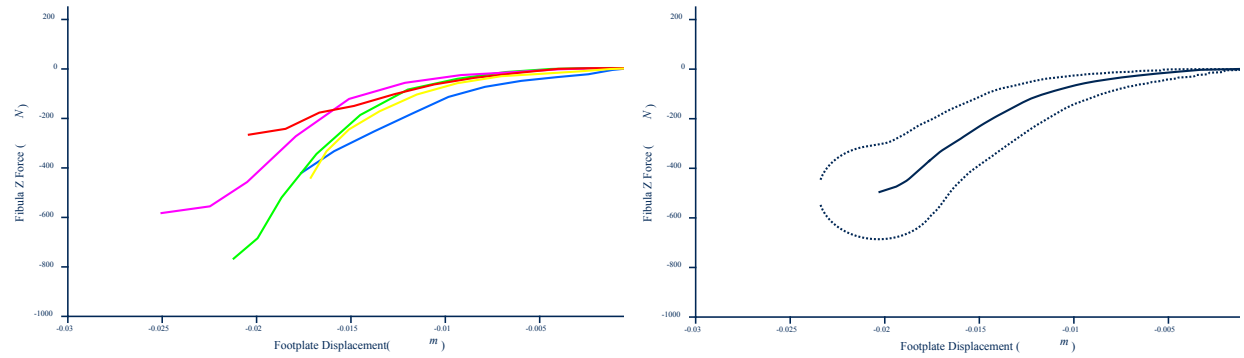

Figure 36. Data traces for the 5 barefoot tests for the axial force measured in the fibula versus footplate displacement (left) and the resulting corridor from those data traces (right).

Total Cross Sectional Combined Tibial and Fibular Load Versus Footplate Displacement

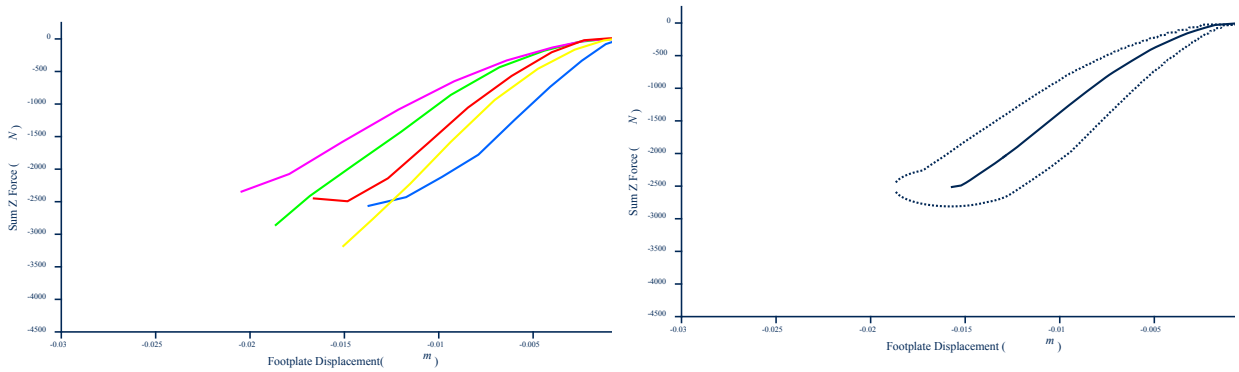

Figure 37. Data traces for the 5 barefoot tests for the axial force combined in the tibia and the fibula versus footplate displacement (left) and the resulting corridor from those data traces (right).

Knee Axial Load Versus Footplate Displacement

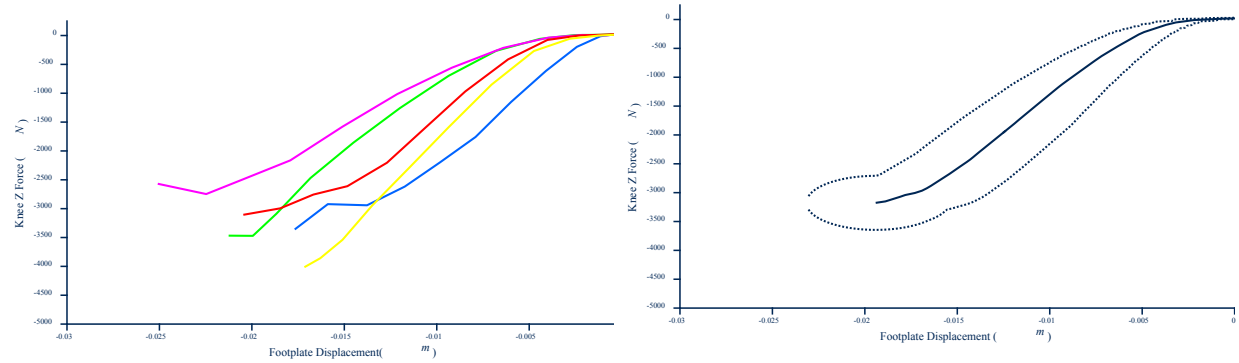

Figure 38. Data traces for the 5 barefoot tests for the axial force measured in the knee load cell versus footplate displacement (left) and the resulting corridor from those data traces (right).

Footplate Axial Load (mass compensated) Versus Footplate Displacement

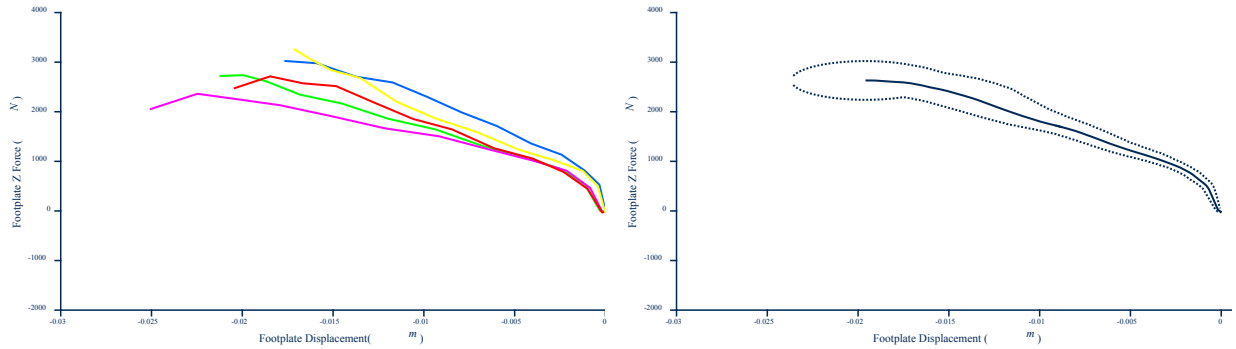

Figure 39. Data traces for the 5 barefoot tests for the axial force calculated in the mass compensated footplate load cell versus footplate displacement (left) and the resulting corridor from those data traces (right).

Results: Scaled Combined Shod and Barefoot Data Corridors Versus Time

Tibia Axial Load Versus Time (scaled by leg length)

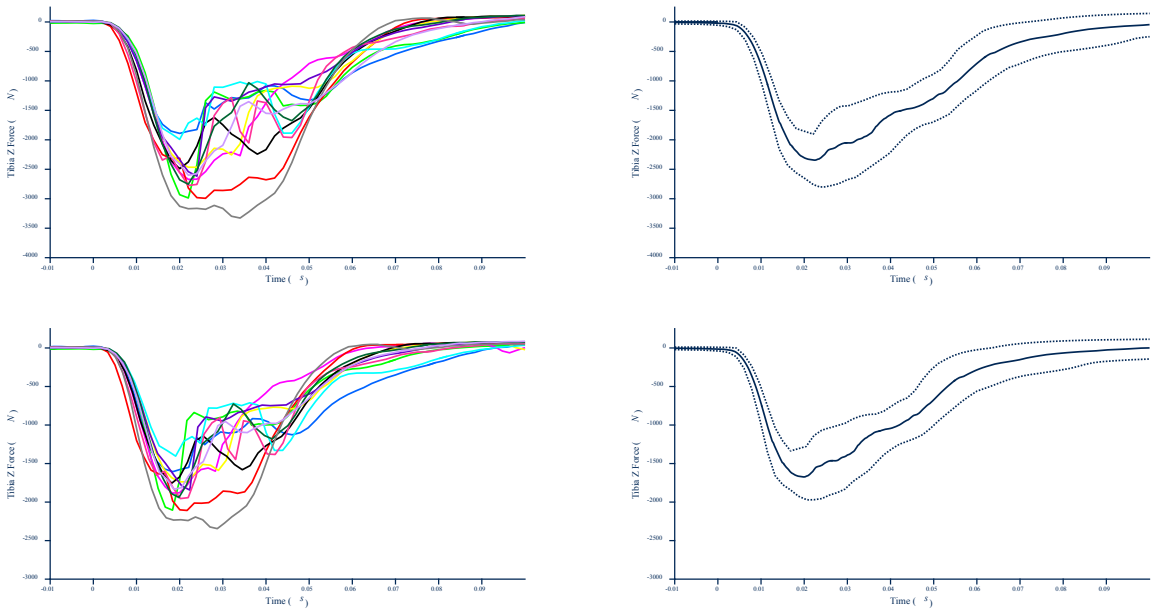

Figure 40. Data traces for the 12 tests for the axial force measured in the tibia versus time (left) and the resulting corridors from those data traces (right). Top plots are the original data, and bottom plots are the data scaled by leg length.

Fibula Axial Load Versus Time (scaled by leg length)

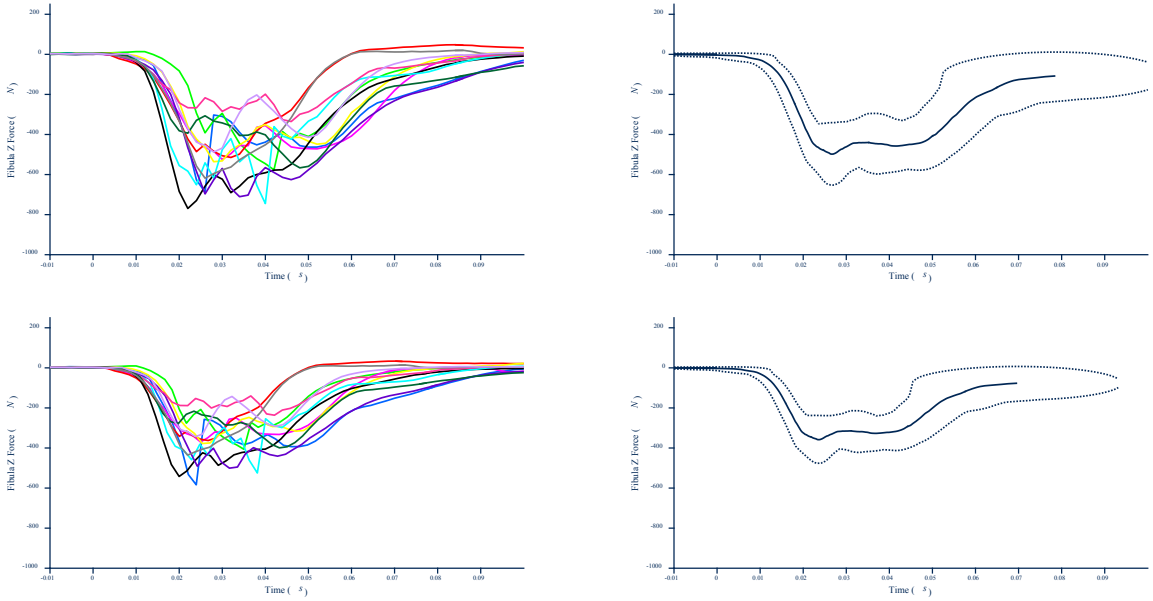

Figure 41. Data traces for the 12 tests for the axial force measured in the fibula versus time (left) and the resulting corridors from those data traces (right). Top plots are the original data, and bottom plots are the data scaled by leg length.

Total Cross Sectional Combined Tibial and Fibular Load Versus Time (scaled by leg length)

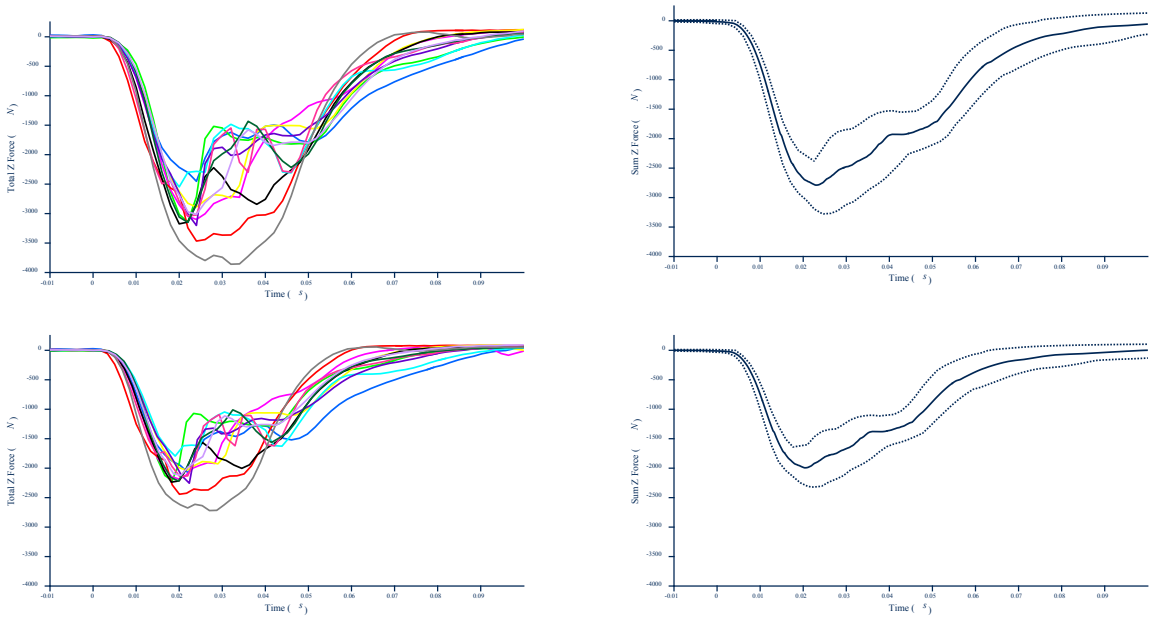

Figure 42. Data traces for the 12 tests for the axial force combined in the tibia and fibula versus time (left) and the resulting corridors from those data traces (right). Top plots are the original data, and bottom plots are the data scaled by leg length.

Knee Axial Load Versus Time (scaled by leg length)

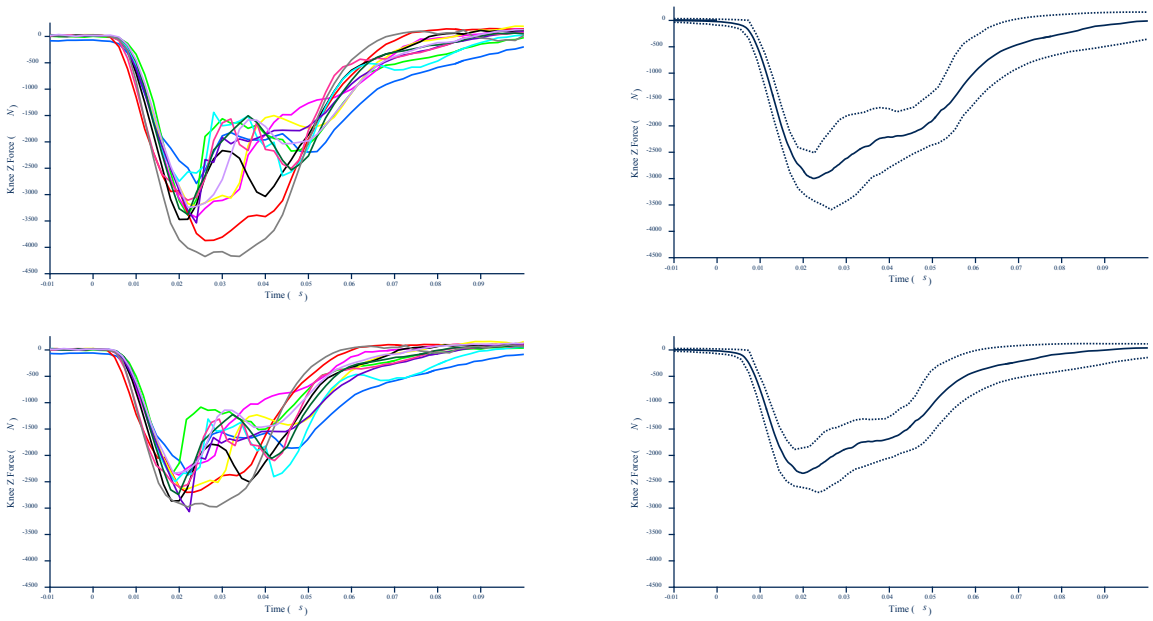

Figure 43. Data traces for the 12 tests for the axial force measured in the knee load cell versus time (left) and the resulting corridors from those data traces (right). Top plots are the original data, and bottom plots are the data scaled by leg length.

Footplate Axial Load (mass compensated) Versus Time (scaled by leg length)

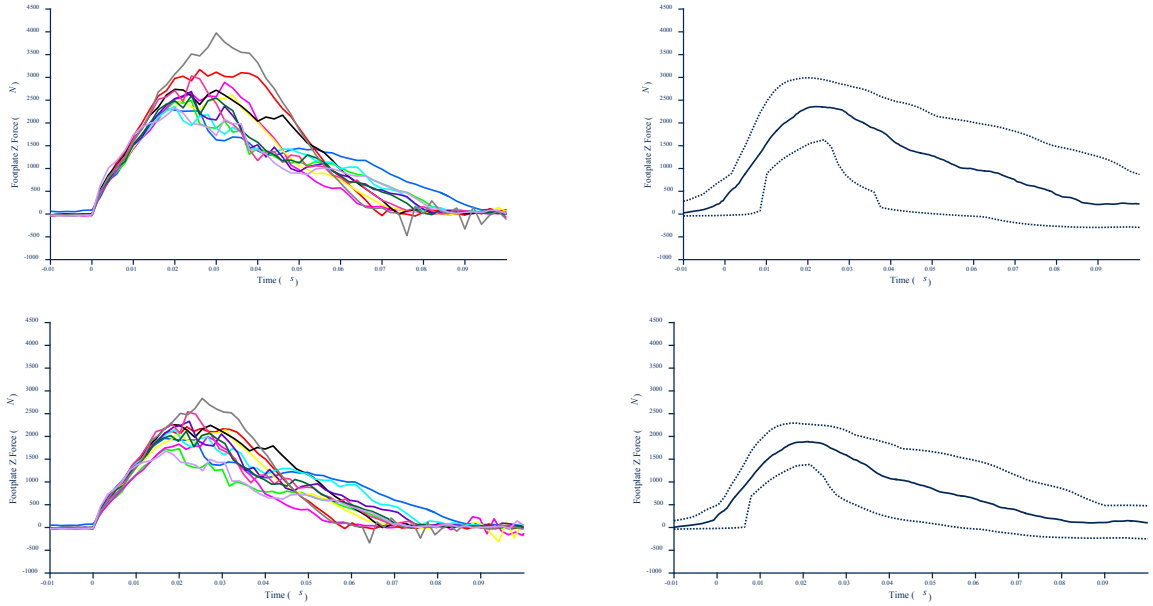

Figure 44. Data traces for the 12 tests for the axial force calculated for the mass compensated footplate load cell versus time (left) and the resulting corridors from those data traces (right). Top plots are the original data, and bottom plots are the data scaled by leg length.

Footplate Displacement Versus Time (scaled by leg length)

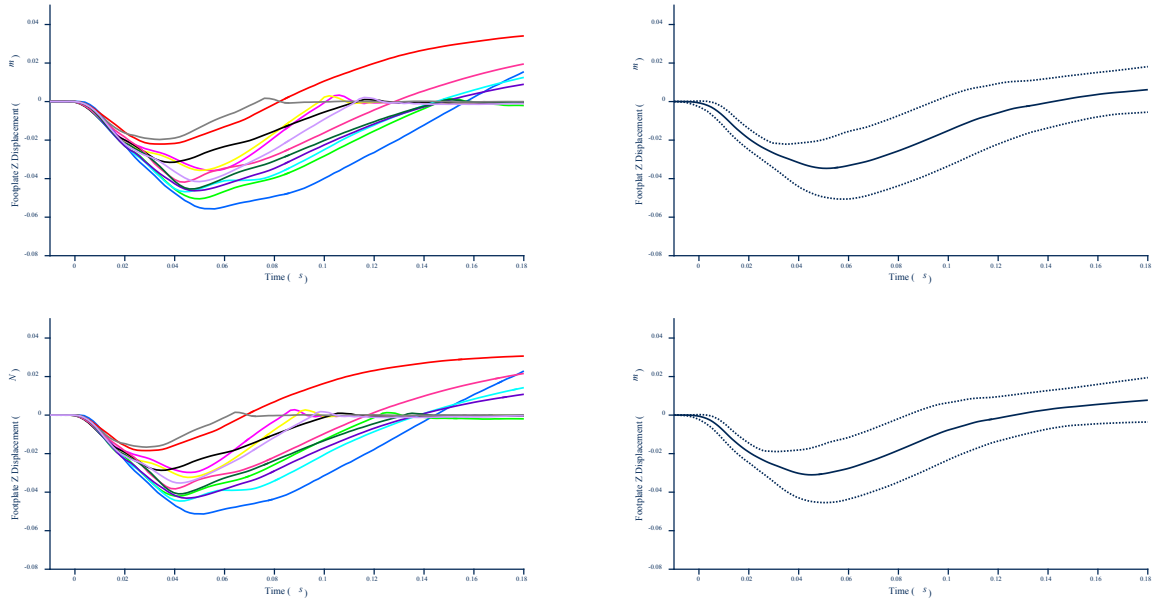

Figure 45. Data traces for all 12 tests for the footplate displacement versus time (left) and the resulting corridors from those data traces (right). Top plots are the original data, and bottom plots are the data scaled by leg length.

Results: Scaled Shod Corridors Versus Time

Tibia Axial Load Versus Time (scaled by leg length)

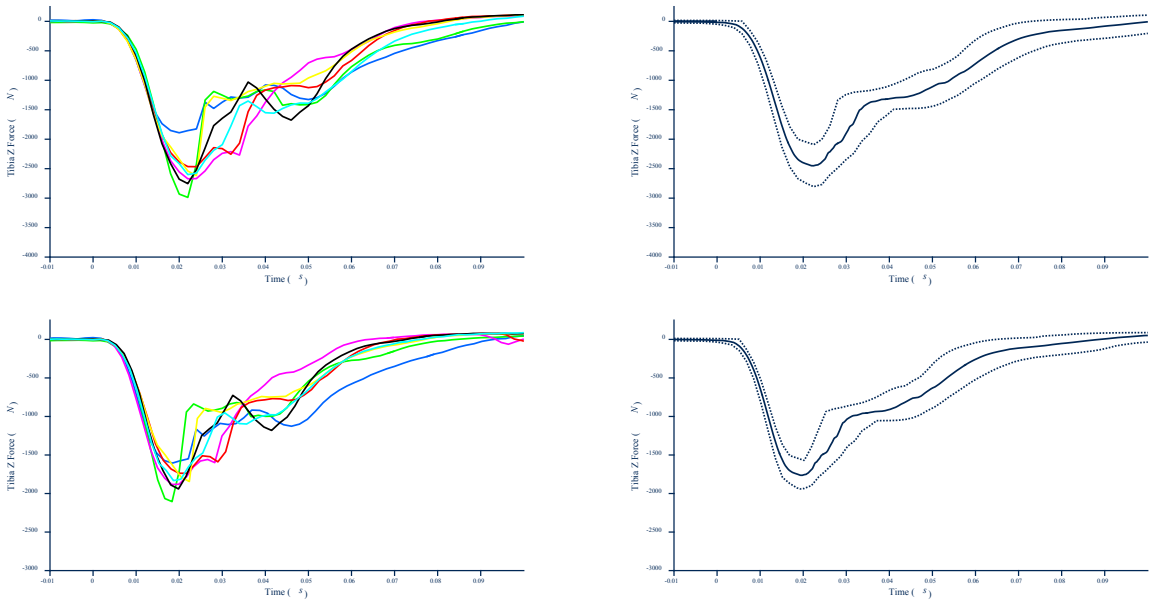

Figure 46. Data traces for the 7 shod tests for the axial force measured in the tibia versus time (left) and the resulting corridors from those data traces (right). Top plots are the original data, and bottom plots are the data scaled by leg length.

Fibula Axial Load Versus Time (scaled by leg length)

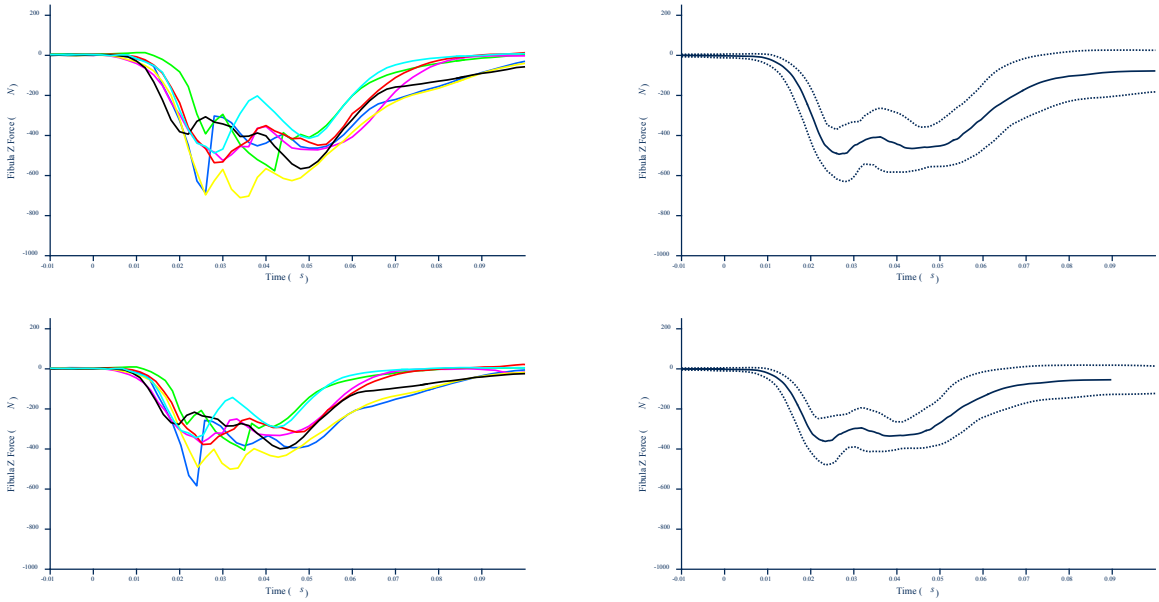

Figure 47. Data traces for the 7 shod tests for the axial force measured in the fibula versus time (left) and the resulting corridors from those data traces (right). Top plots are the original data, and bottom plots are the data scaled by leg length.

Total Cross Sectional Combined Tibial and Fibular Load Versus Time (scaled by leg length)

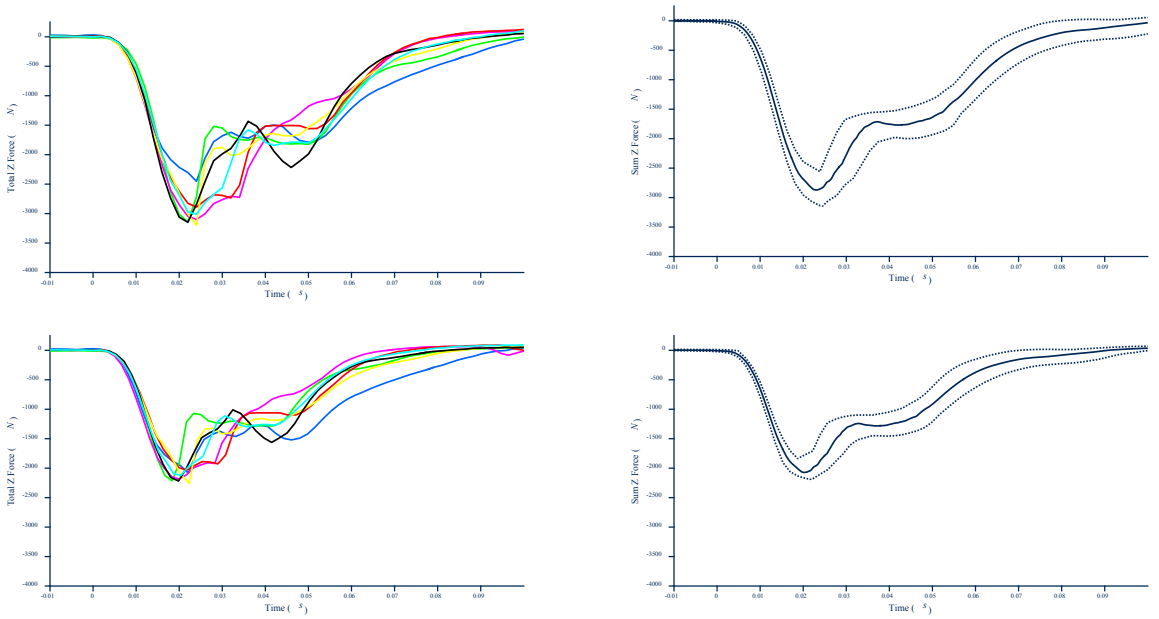

Figure 48. Data traces for the 7 shod tests for the axial force combined in the tibia and fibula versus time (left) and the resulting corridors from those data traces (right). Top plots are the original data, and bottom plots are the data scaled by leg length.

Knee Axial Load Versus Time (scaled by leg length)

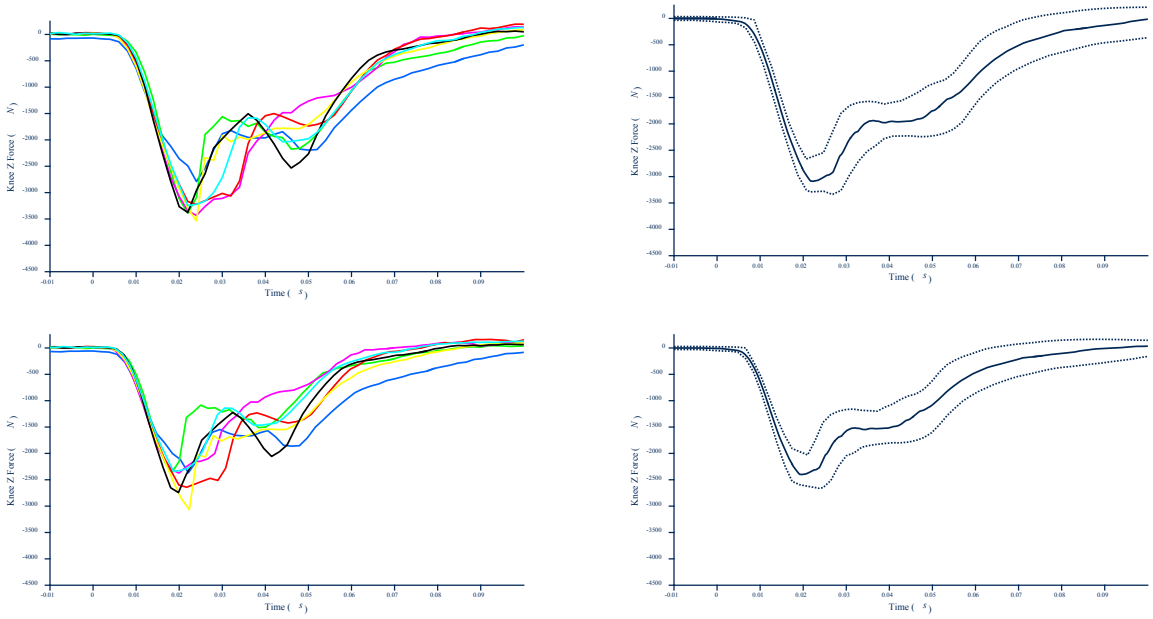

Figure 49. Data traces for the 7 shod tests for the axial force measured in the knee load cell versus time (left) and the resulting corridors from those data traces (right). Top plots are the original data, and bottom plots are the data scaled by leg length.

Footplate Axial Load (mass compensated) Versus Time (scaled by leg length)

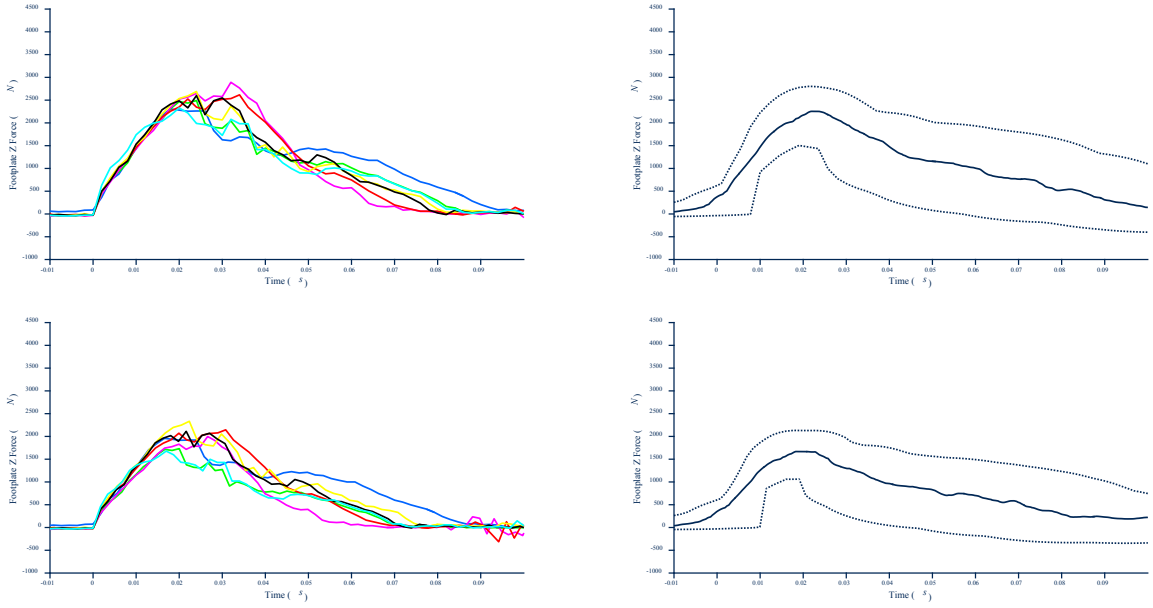

Figure 50. Data traces for the 7 shod tests for the axial force calculated from the mass compensated footplate load cell versus time (left) and the resulting corridors from those data traces (right). Top plots are the original data, and bottom plots are the data scaled by leg length.

Footplate Displacement Versus Time (scaled by leg length)

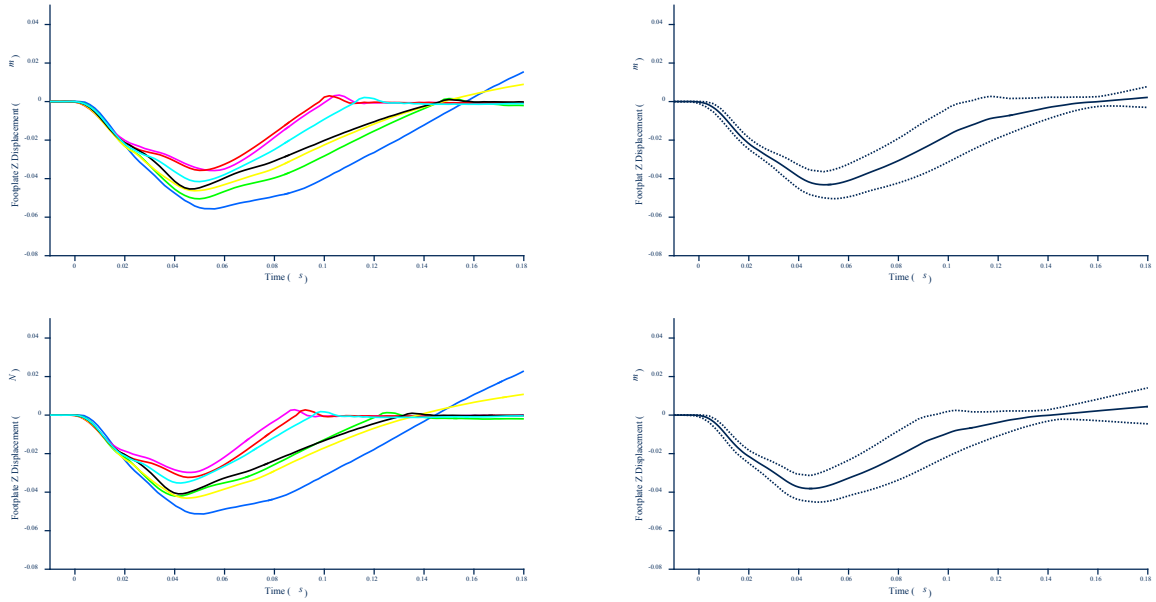

Figure 51. Data traces for the 7 shod tests for the footplate displacement versus time (left) and the resulting corridors from those data traces (right). Top plots are the original data, and bottom plots are the data scaled by leg length.

Results: Scaled Barefoot Corridors Versus Time

Tibia Axial Load Versus Time (scaled by leg length)

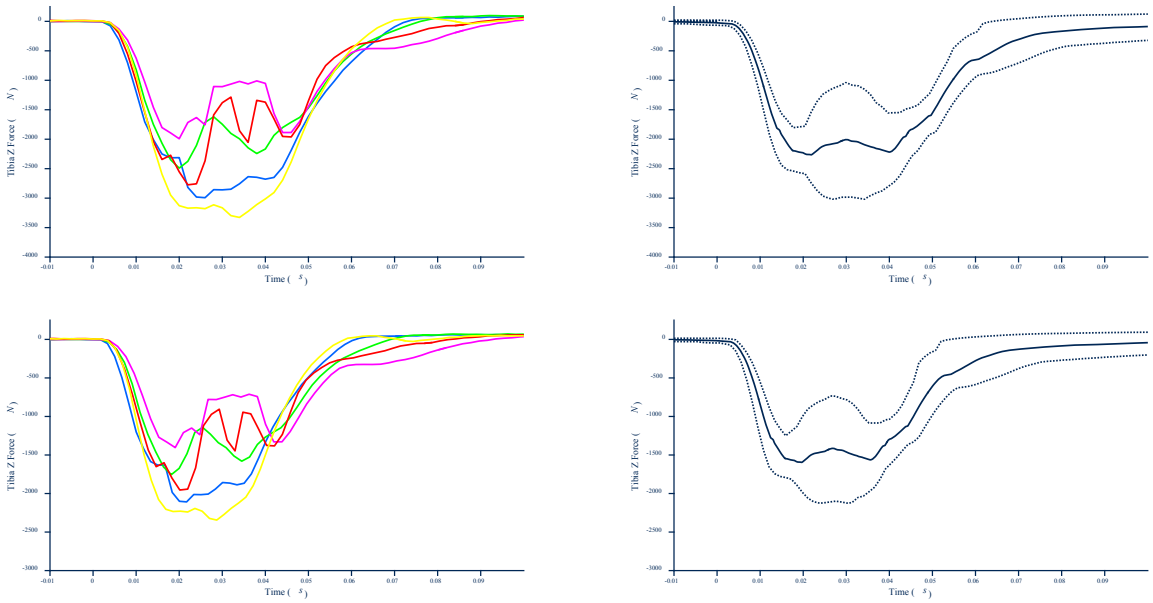

Figure 52. Data traces for the 5 barefoot tests for the axial force measured in the tibia versus footplate displacement (left) and the resulting corridors from those data traces (right). Top plots are the original data, and bottom plots are the data scaled by leg length.

Fibula Axial Load Versus Time (scaled by leg length)

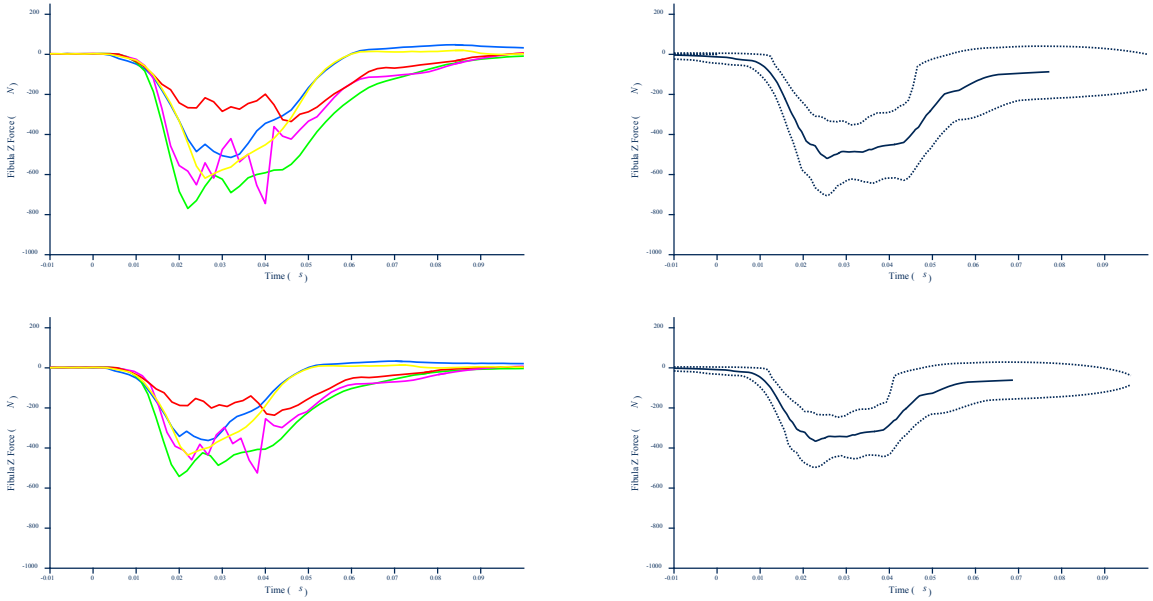

Figure 53. Data traces for the 5 barefoot tests for the axial force measured in the fibula versus time (left) and the resulting corridors from those data traces (right). Top plots are the original data, and bottom plots are the data scaled by leg length.

Total Cross Sectional Combined Tibial and Fibular Load Versus Time (scaled by leg length)

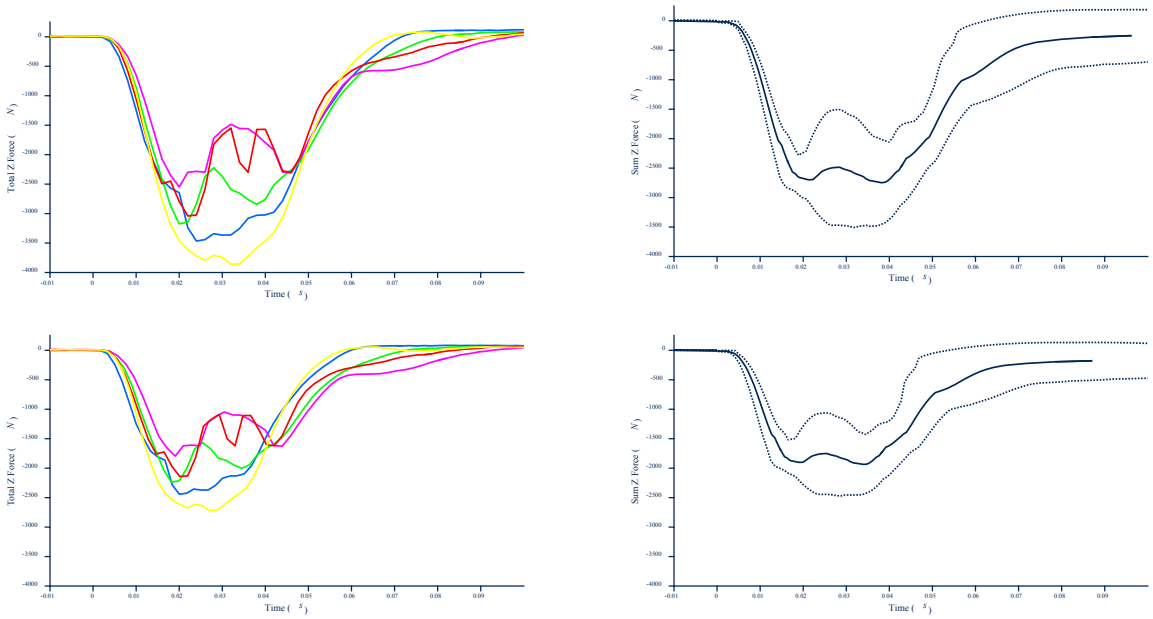

Figure 54. Data traces for the 5 barefoot tests for the axial force combined in the tibia and fibula versus time (left) and the resulting corridors from those data traces (right). Top plots are the original data, and bottom plots are the data scaled by leg length.

Knee Axial Load Versus Time (scaled by leg length)

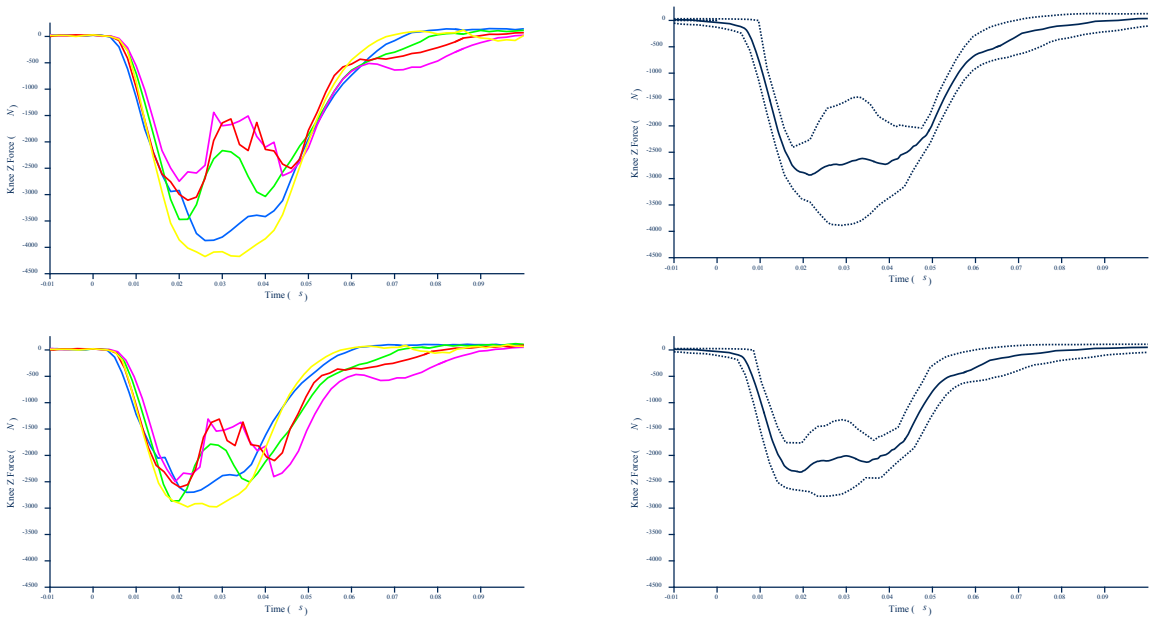

Figure 55. Data traces for the 5 barefoot tests for the axial force measured in the knee load cell versus time (left) and the resulting corridors from those data traces (right). Top plots are the original data, and bottom plots are the data scaled by leg length.

Footplate Axial Load (mass compensated) Versus Time (scaled by leg length)

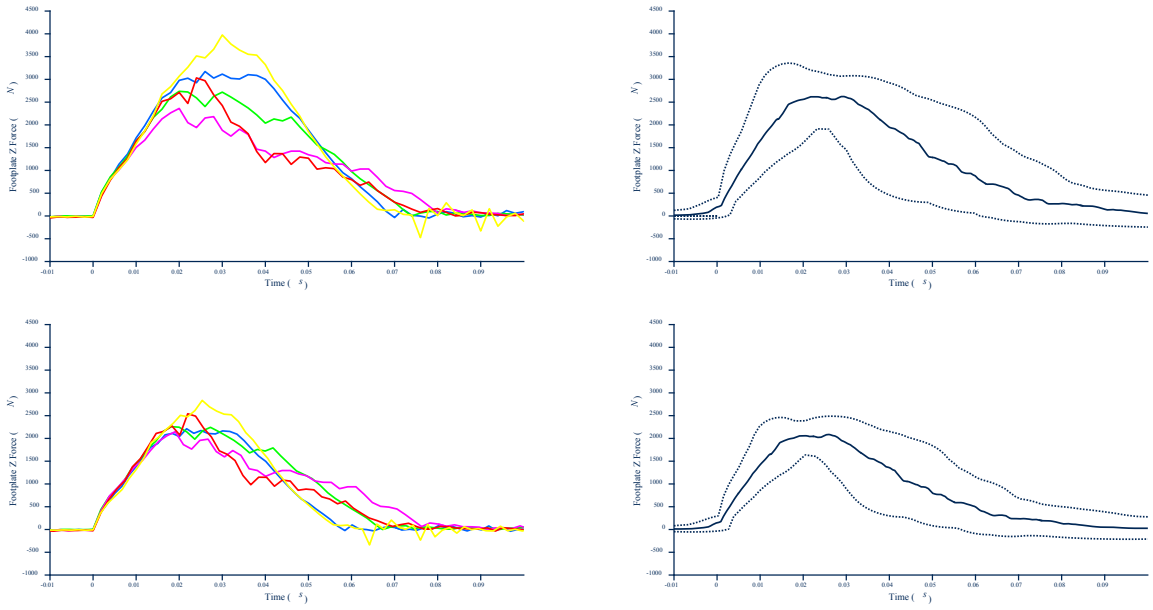

Figure 56. Data traces for the 5 barefoot tests for the axial force calculated using mass compensation of the footplate load cell versus time (left) and the resulting corridors from those data traces (right). Top plots are the original data, and bottom plots are the data scaled by leg length.

Footplate Displacement Versus Time (scaled by leg length)

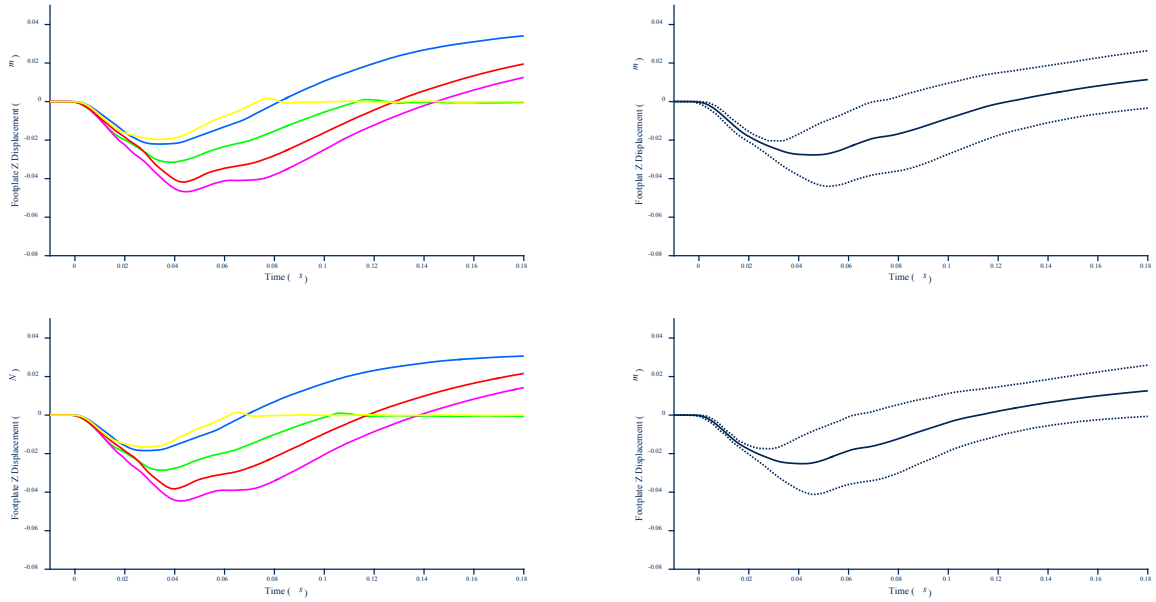

Figure 57. Data traces for the 5 barefoot tests for the footplate displacement versus time (left) and the resulting corridors from those data traces (right). Top plots are the original data, and bottom plots are the data scaled by leg length.

Results: Scaled Combined Shod and Barefoot Data Corridors Versus Displacement

Tibia Axial Load Versus Footplate Displacement (scaled by leg length)

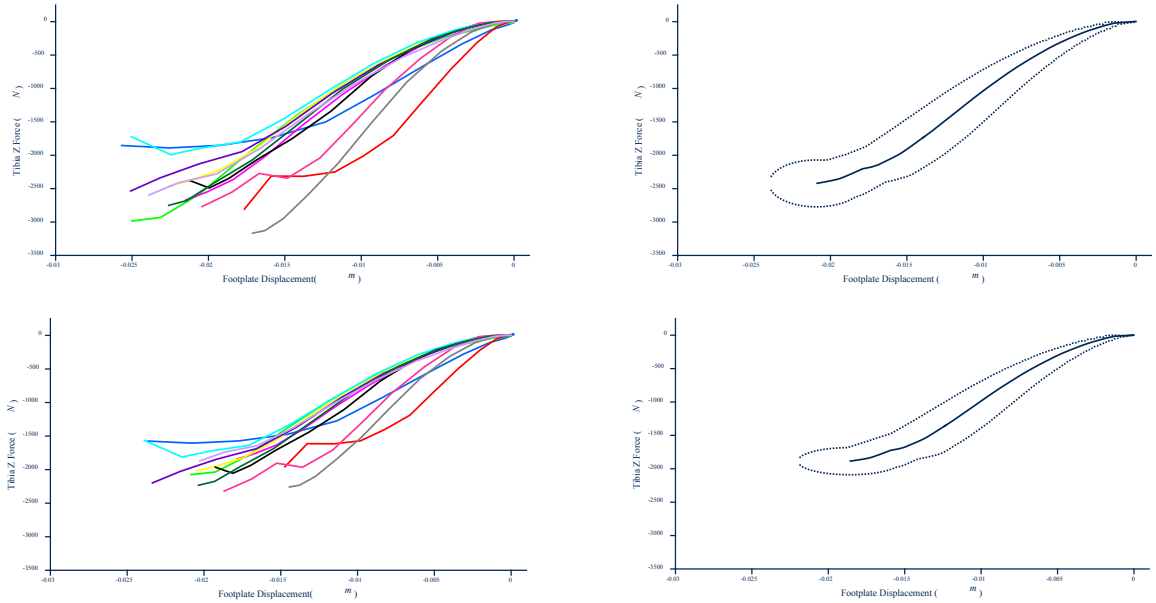

Figure 58. Data traces for the 12 tests for the axial force measured in the tibia versus footplate displacement (left) and the resulting corridors from those data traces (right). Top plots are the original data, and bottom plots are the data scaled by leg length.

Fibula Axial Load Versus Footplate Displacement (scaled by leg length)

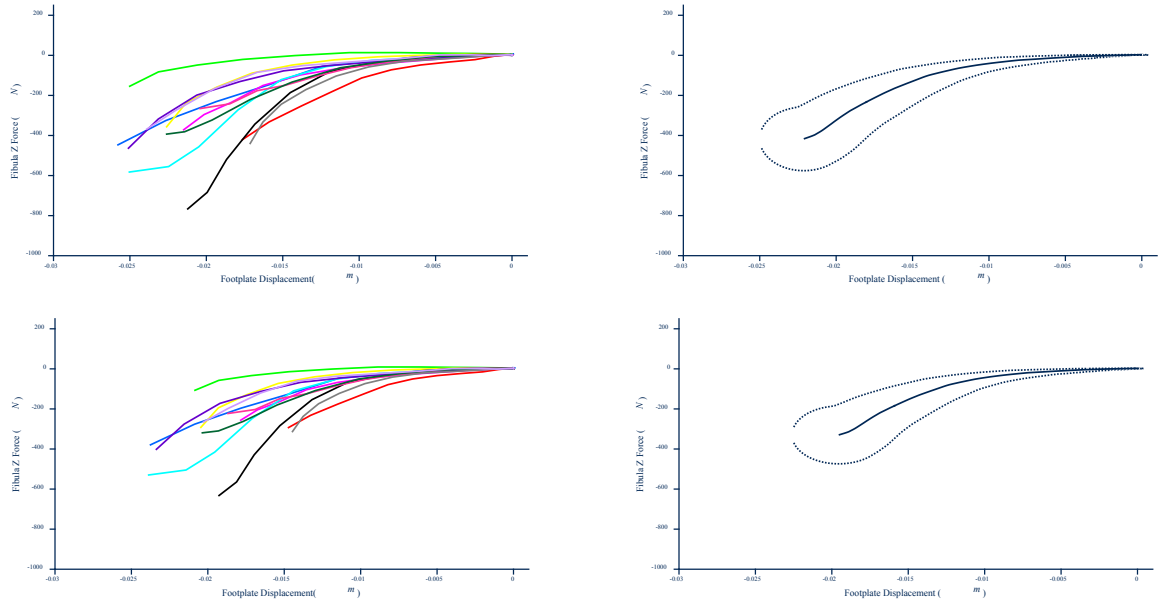

Figure 59. Data traces for the 12 tests for the axial force measured in the fibula versus footplate displacement (left) and the resulting corridors from those data traces (right). Top plots are the original data, and bottom plots are the data scaled by leg length.

Total Combined Tibial and Fibular Load Versus Footplate Displacement (scaled by leg length)

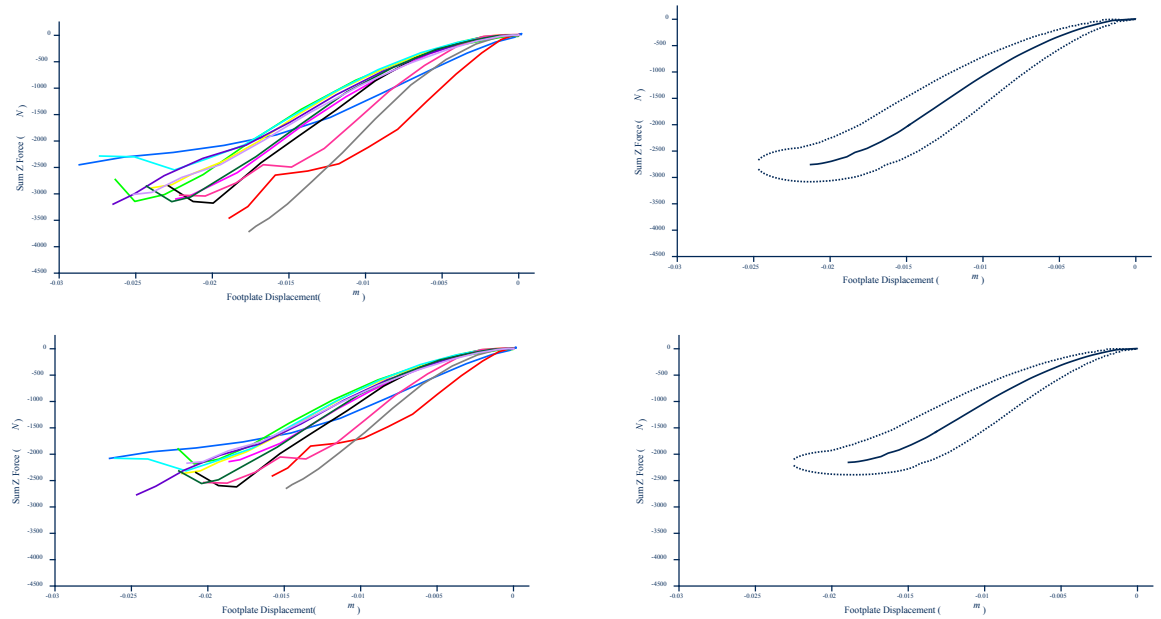

Figure 60. Data traces for the 12 tests for the axial force combined in the tibia and fibula versus footplate displacement (left) and the resulting corridors from those data traces (right). Top plots are the original data, and bottom plots are the data scaled by leg length.

Knee Axial Load Versus Footplate Displacement (scaled by leg length)

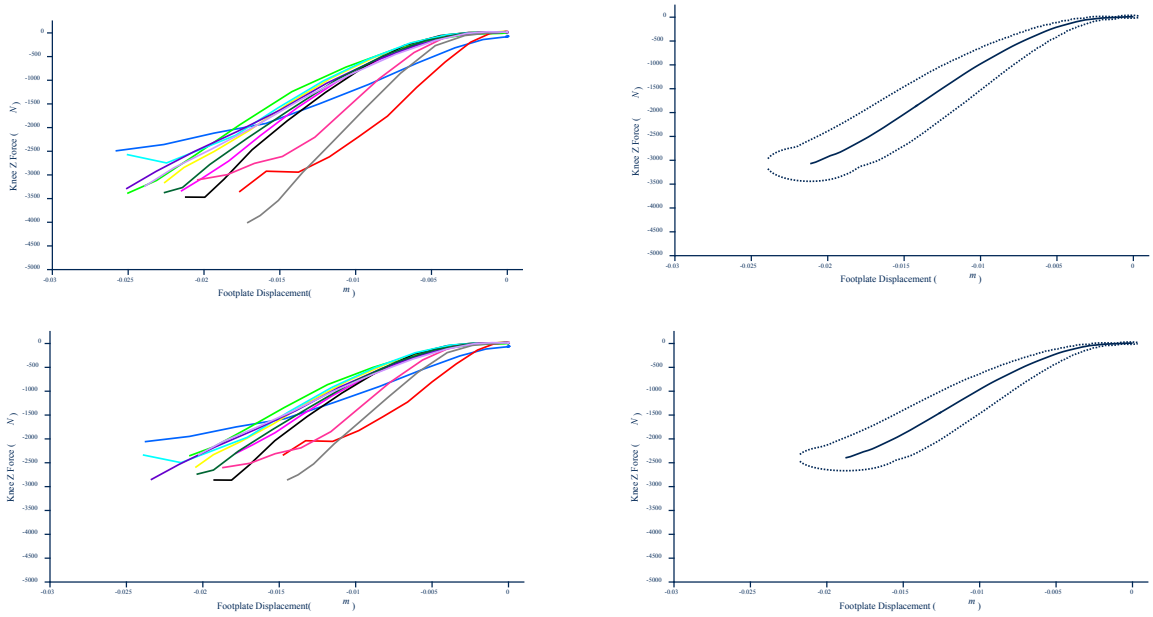

Figure 61. Data traces for the 12 tests for the axial force measured in the knee load cell versus footplate displacement (left) and the resulting corridors from those data traces (right). Top plots are the original data, and bottom plots are the data scaled by leg length.

Footplate Axial Load (mass compensated) Versus Footplate Displacement (scaled by leg length)

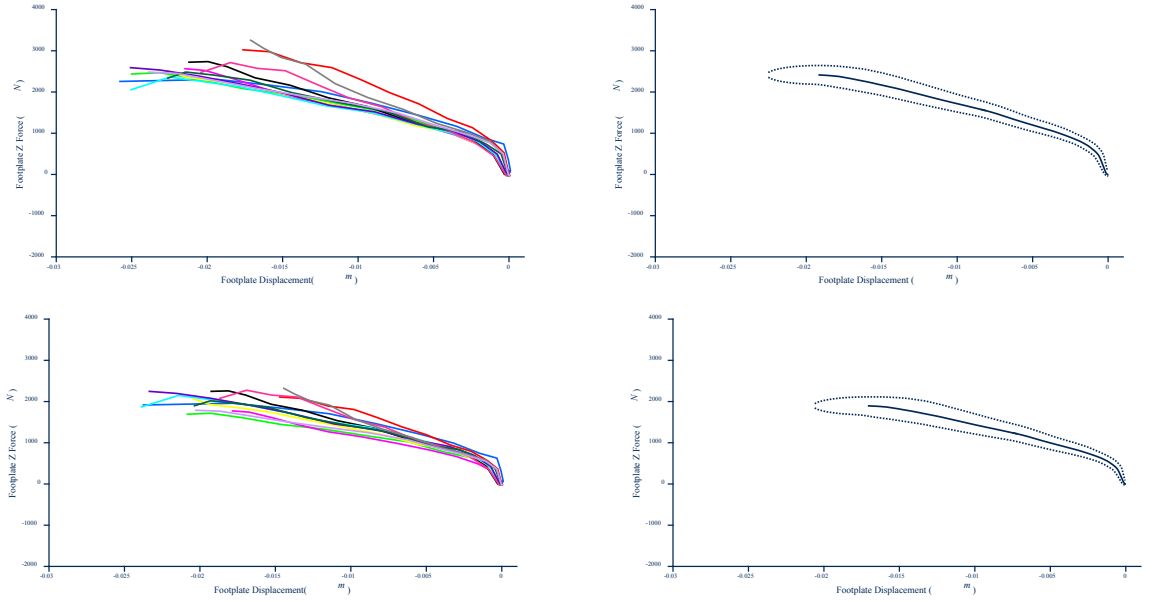

Figure 62. Data traces for the 12 tests for the axial force calculated from the mass compensated footplate load cell versus footplate displacement (left) and the resulting corridors from those data traces (right). Top plots are the original data, and bottom plots are the data scaled by leg length.

Results: Scaled Shod Data Corridors Versus Displacement

Tibia Axial Load Versus Footplate Displacement (scaled by leg length)

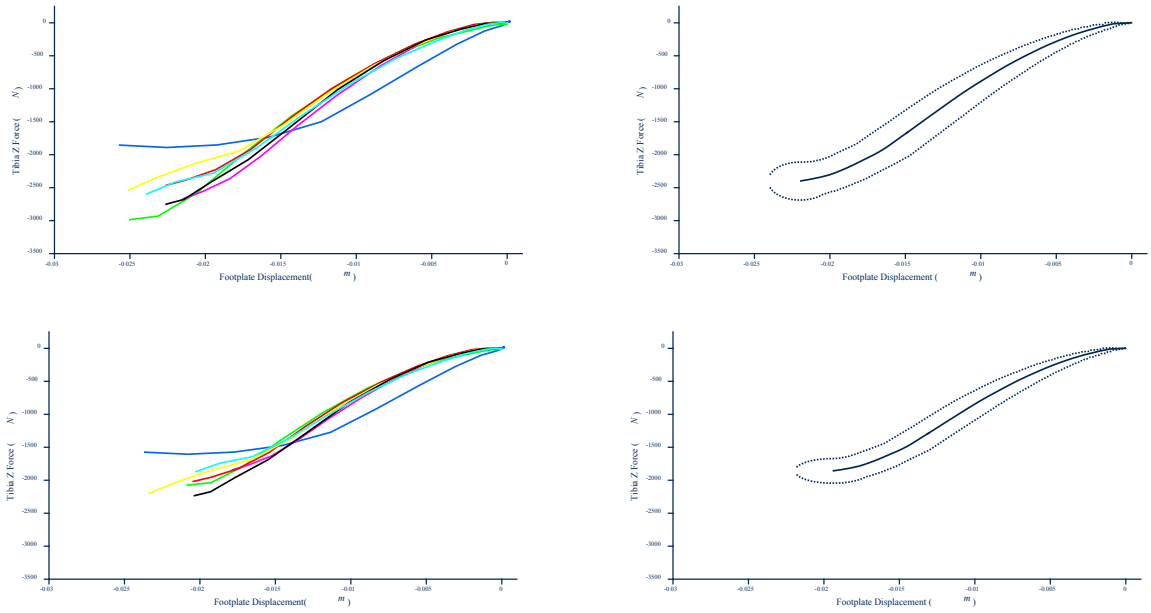

Figure 63. Data traces for the 7 shod tests for the axial force measured in the tibia versus footplate displacement (left) and the resulting corridors from those data traces (right). Top plots are the original data, and bottom plots are the data scaled by leg length.

Fibula Axial Load Versus Footplate Displacement (scaled by leg length)

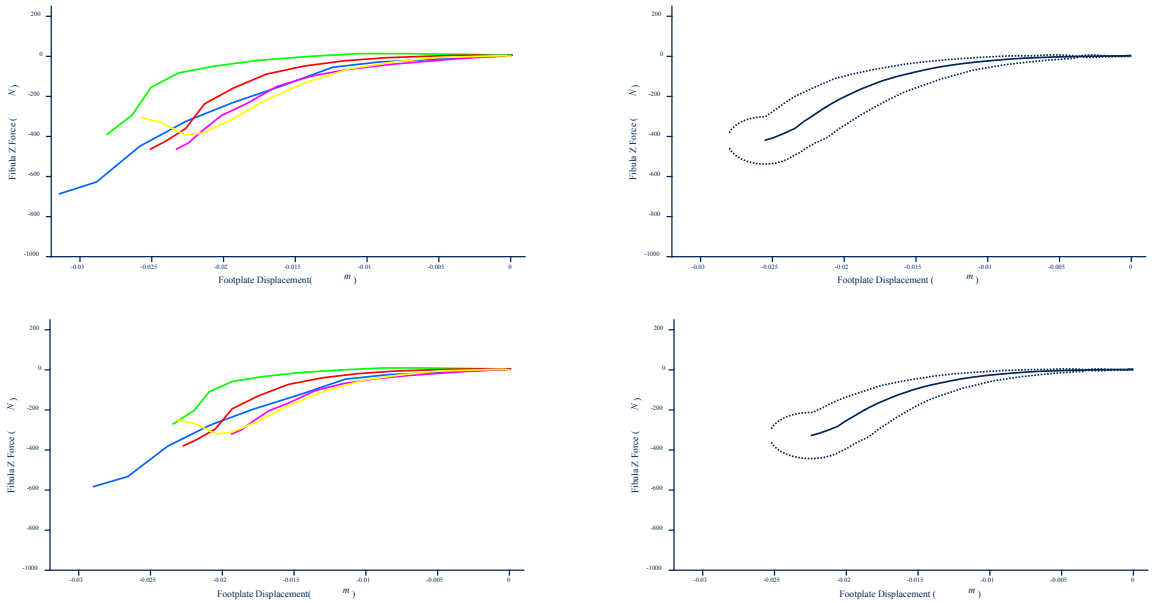

Figure 64. Data traces for the 7 shod tests for the axial force measured in the fibula versus footplate displacement (left) and the resulting corridors from those data traces (right). Top plots are the original data, and bottom plots are the data scaled by leg length.

Total Cross Sectional Combined Tibial and Fibular Load Versus Footplate Displacement (scaled by leg length)

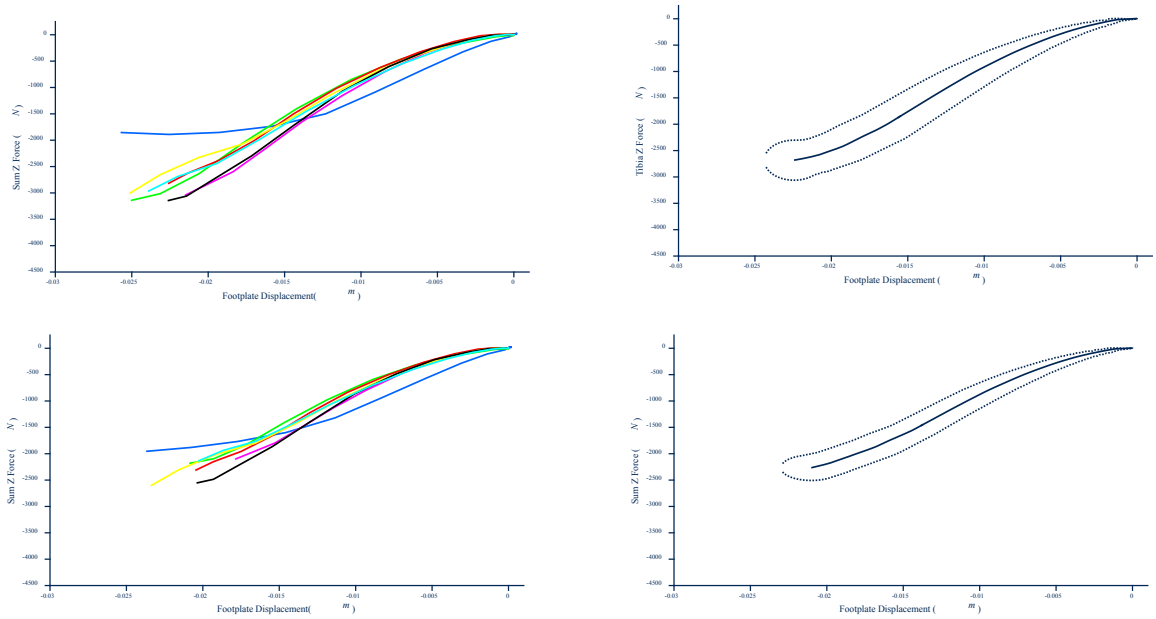

Figure 65. Data traces for the 7 shod tests for the axial force combined in the tibia and fibula versus footplate displacement (left) and the resulting corridors from those data traces (right). Top plots are the original data, and bottom plots are the data scaled by leg length.

Knee Axial Load Versus Footplate Displacement (scaled by leg length)

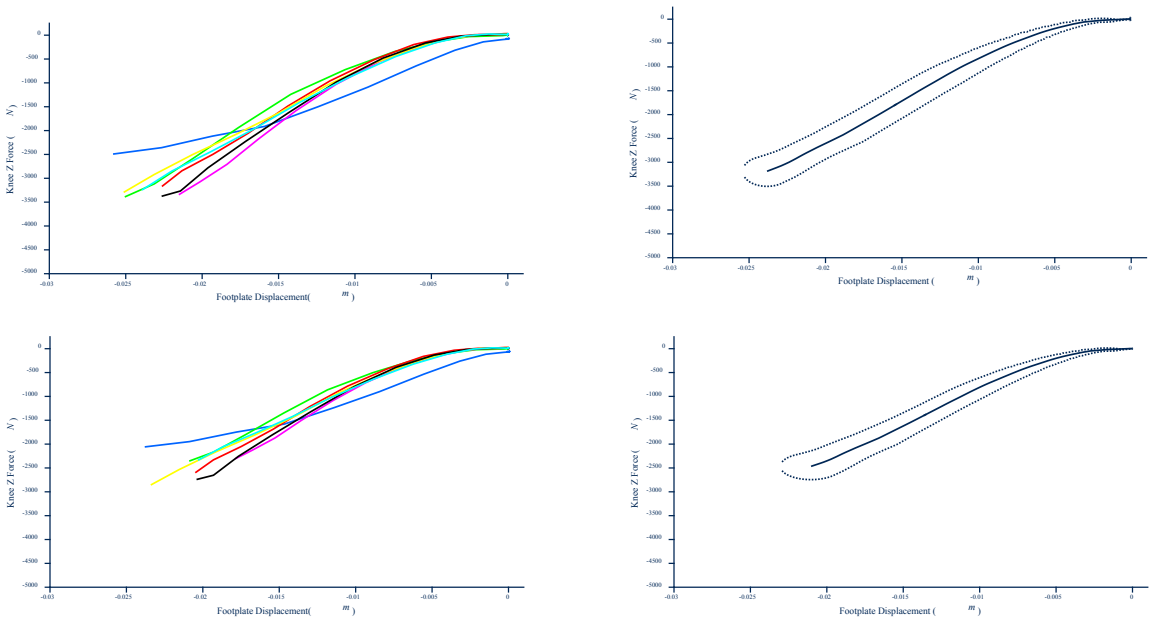

Figure 66. Data traces for the 7 shod tests for the axial force measured in the knee load cell versus footplate displacement (left) and the resulting corridors from those data traces (right). Top plots are the original data, and bottom plots are the data scaled by leg length.

Footplate Axial Load (mass compensated) Versus Footplate Displacement (scaled by leg length)

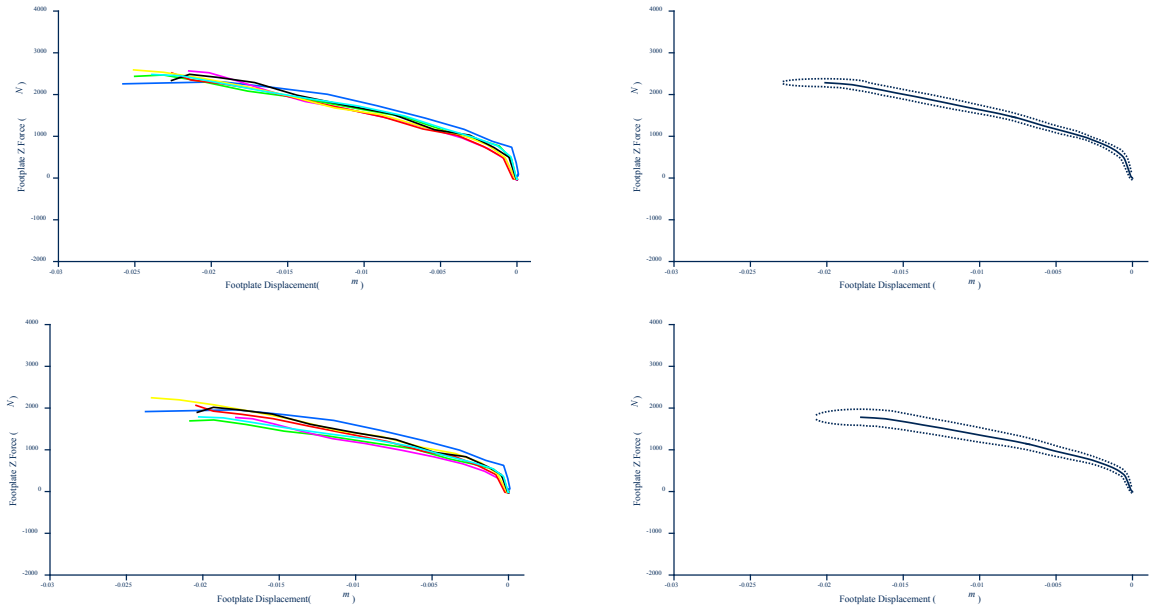

Figure 67. Data traces for the 7 shod tests for the axial force calculated from the mass compensated footplate load cell versus footplate displacement (left) and the resulting corridors from those data traces (right). Top plots are the original data, and bottom plots are the data scaled by leg length.

Results: Scaled Barefoot Data Corridors Versus Displacement

Tibia Axial Load Versus Footplate Displacement (scaled by leg length)

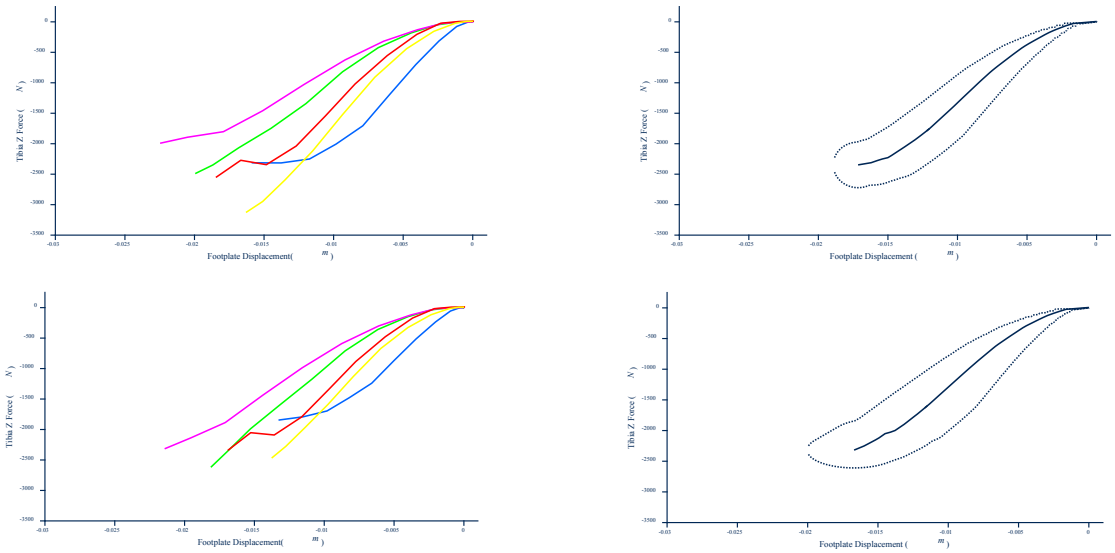

Figure 68. Data traces for the 5 barefoot tests for the axial force measured in the tibia versus footplate displacement (left) and the resulting corridors from those data traces (right). Top plots are the original data, and bottom plots are the data scaled by leg length.

Fibula Axial Load Versus Footplate Displacement (scaled by leg length)

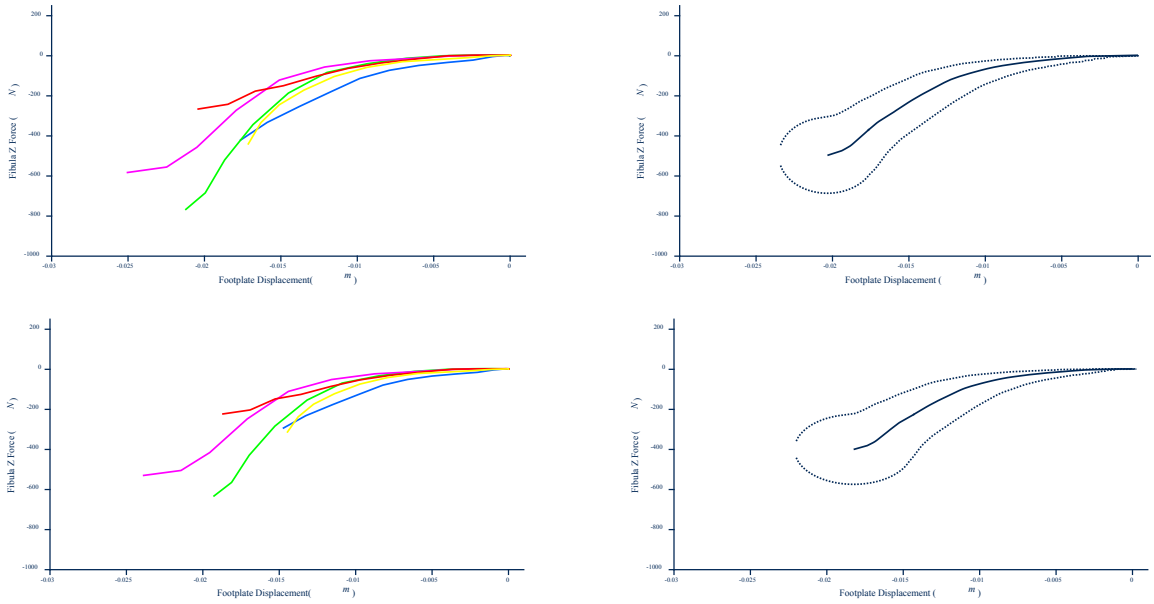

Figure 69. Data traces for the 5 barefoot tests for the axial force measured in the fibula versus footplate displacement (left) and the resulting corridors from those data traces (right). Top plots are the original data, and bottom plots are the data scaled by leg length.

Total Combined Tibial and Fibular Load Versus Footplate Displacement (scaled by leg length)

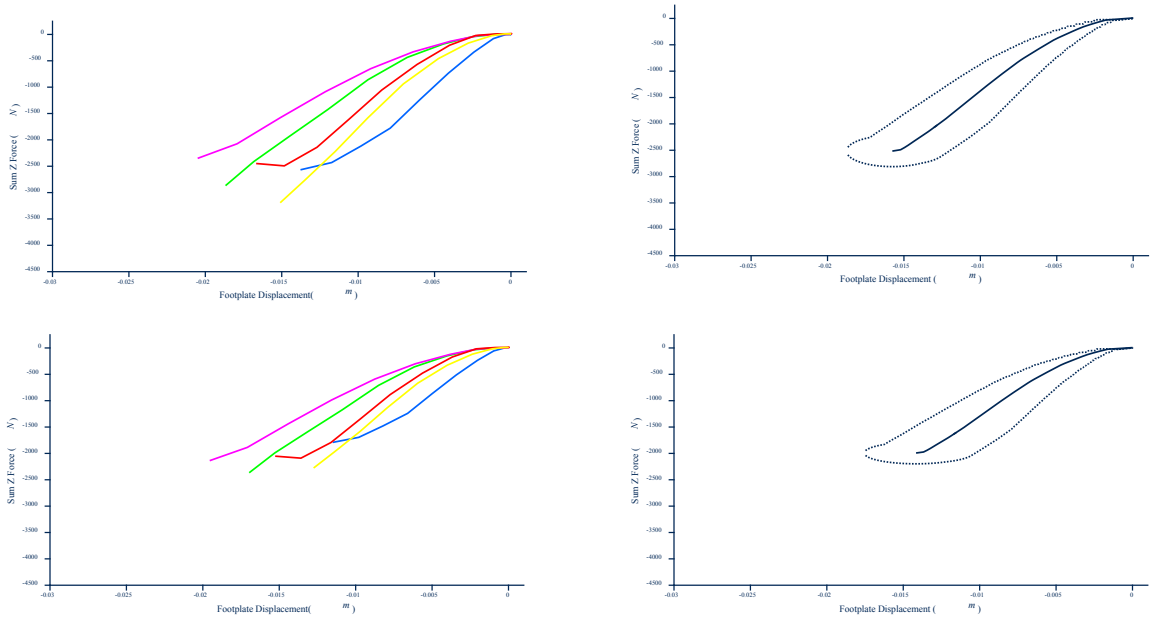

Figure 70. Data traces for the 5 barefoot tests for the axial force combined in the tibia and fibula versus footplate displacement (left) and the resulting corridors from those data traces (right). Top plots are the original data, and bottom plots are the data scaled by leg length.

Knee Axial Load Versus Footplate Displacement (scaled by leg length)

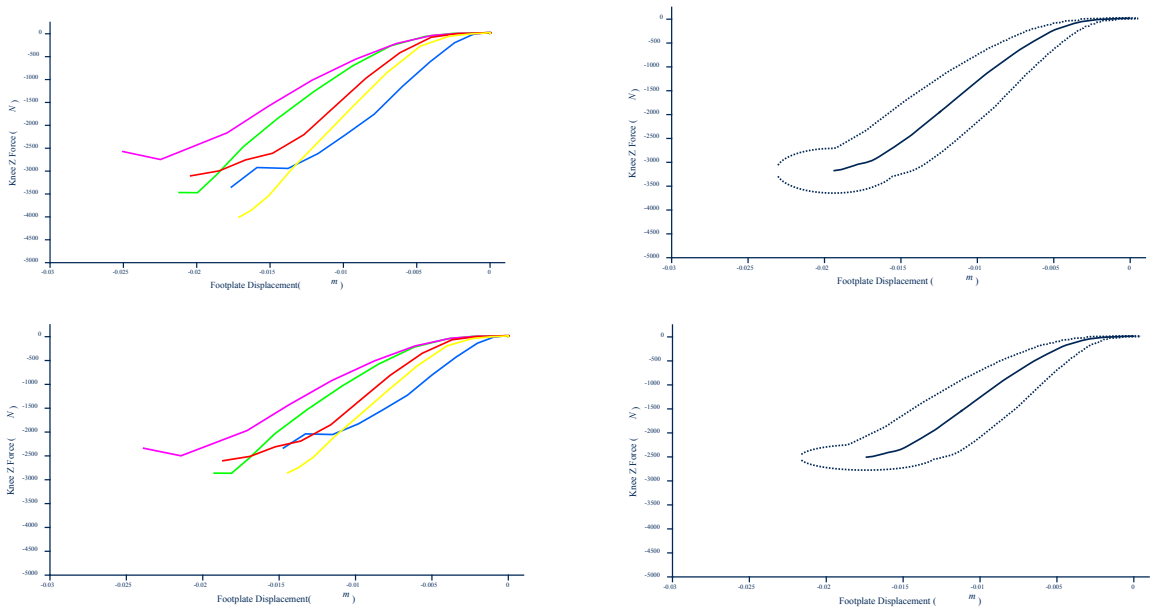

Figure 71. Data traces for the 5 barefoot tests for the axial force measured in the knee load cell versus footplate displacement (left) and the resulting corridors from those data traces (right). Top plots are the original data, and bottom plots are the data scaled by leg length.

Footplate Axial Load (mass compensated) Versus Footplate Displacement (scaled by leg length)

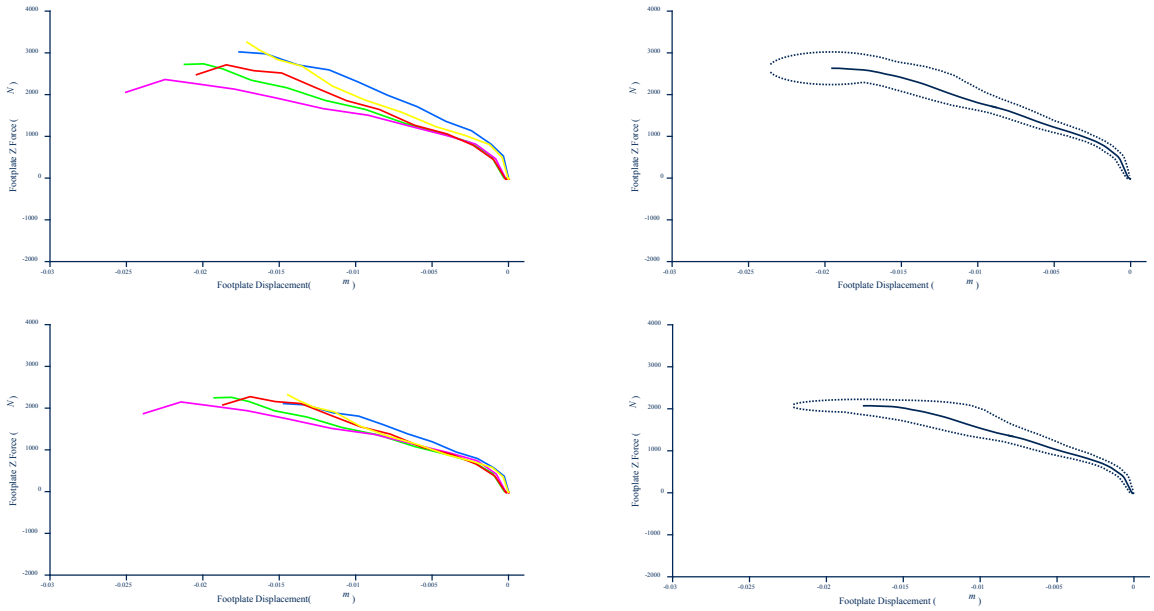

Figure 72. Data traces for the 5 barefoot tests for the axial force calculated from the mass compensated footplate load cell versus footplate displacement (left) and the resulting corridors from those data traces (right). Top plots are the original data, and bottom plots are the data scaled by leg length.

Recommendations and Use of Biofidelity Corridors for ATDs

To use these corridors for biofidelity evaluation of a 5th percentile female ATD, leg-length scaled corridors formed with shod data are recommended for use. Given that most modern ATDs have a molded shoe, or are tested while wearing a shoe, and that there were differences between the shod and barefoot corridors, it makes the most sense to use shod data as the dataset to predict response. Scaled corridors are recommended because internal axial load measurements have been found to vary with differences in gross anthropometry metrics such as height and total mass, and all the specimens tested in this series were larger than the 5th percentile female target anthropometry. Figures for these corridors can be found in the following two sections: "Results: Scaled Shod Data Corridors Versus Time" and "Results: Scaled Shod Data Corridors Versus Displacement".

Given than most ATDs have one load cell to representing the load supported by both the tibia and fibula, "Total Combined Tibial and Fibular Load" corridors should be used to evaluate ATD biofidelity. It should also be noted that it is unlikely that a load cell in an ATD will be in the exact same location as the origin of the anatomic coordinate system created in the corridor development. It is necessary to transform the forces of the biofidelity corridors created in for the tibia and fibula load cell (and combined tibia and fibula load) in this document to the ATD load cell coordinate system, to properly evaluate how the forces measured internal to the ATD correspond the biofidelity corridors. These transformations can be accomplished using the same matrix equations in the section of this document titled "Transformation of Load Cell Data to be aligned with Anatomic Coordinate System," but instead of transforming between the "load cell coordinate system" to the "anatomic coordinate system," the corridor data must be transformed from the "anatomic coordinate system" to the "ATD load cell coordinate system." In other words, a transformation matrix must be created relating the "anatomic coordinate system" defined in this text, and the coordinate system of the load cell internal to the ATD being evaluated.

Because the footplate displacement, footplate axial load, and knee axial load are measurements made on the external test fixture, they should be compared to external measured values in ATD tests, comparable to this test setup. It should not be assumed that an axial knee force measured inside an ATD would be equivalent to the response of the external knee load cell.

Conclusions

This report details the methodology in the creation of biofidelity corridors that correspond to the a 5th female ATD lower extremity based on a series of small female axial loading tests performed at UVA CAB. Corridors reported include time-history data (footplate displacement, footplate axial load, combined cross sectional axial load from the tibia and fibula load cells, tibia axial load, fibula axial load, and knee axial load), cross plotted responses with footplate displacement (footplate axial load, combined cross sectional axial load from the tibia and fibula load

cells, tibia axial load, fibula axial load, and knee axial load), and corridors developed from leg length scaled data.

Shod corridors (employing leg-length scaling) are recommended as the response targets for a shod 5th percentile female dummy lower extremity, and recommendations for use of these corridors with ATDs are detailed in this report.

References

Ash, J. H., Lessley, D. J., Forman, J. L., Zhang, Q., Shaw, C. G., & Crandall, J. R. (2012). Whole-body kinematics: response corridors for restrained PMHS in frontal impacts. In *Proceedings of the 2012 International IRCOBI Conference on the Biomechanics of Injury*, September 12-14, Dublin, Ireland, pp. 142-154.

Donlon, J.-P., Joodaki, H., Toczyski, J., Lessley, D. J., & Forman, J. L. (2016). Biofidelity corridors using arc-length parameterization. In *Proceedings from the 44th International Workshop on Human Subjects for Biomechanical Research*, November 5, 2016, Washington, DC.

Eppinger, R. H. (1976). Prediction of thoracic injury using measurable experimental parameters. In *Proceedings of the 6th International Technical Conference on Experimental Safety Vehicles, October 12-15, 1976, ,* Washington, DC, pp. 770-780.

Funk, J. R., Crandall, J. R., Tourret, L. J., MacMahon, C. B., Bass, C. R., Patrie, J. T., … Eppinger, R. H. (2002). The axial injury tolerance of the human foot/ankle complex and the effect of Achilles tension. *Journal of biomechanical engineering, 124*, no. 6: 750-757.

Hollister, A. M., Jatana, S., Singh, A. K., Sullivan, W. W., & Lupichuk, A. G. (1993). The axes of rotation of the knee. *Clinical orthopaedics and related research, 290*: 259-268.

Kerrigan, J. R., Drinkwater, D. C., Kam, C. Y., Murphy, D. B., Ivarsson, B. J., Crandall, J. R., Patrie, J. (2004). Tolerance of the human leg and thigh in dynamic latero-medial bending. *International journal of crashworthiness,* 9, no. 6: 607-623.

Kuppa, S., Wang, J., Haffner, M., & Eppinger, R. (2001). "Lower extremity injuries and associated injury criteria. In *Proceedings of the 17th International Technical Conference on the Enhanced Safety of Vehicles, June 4-7, 2001; Amsterdam, The Netherlands,*Paper no. 457.

Lundberg, A., Svensson, O. K., Nemeth, G., & Selvik, G. (1989). The axis of rotation of the ankle joint. *Bone & Joint Journal, 71*, no. 1: 94-99.

Untaroiu, C., Shin, J., Ivarsson, J., Crandall, J., Takahashi, Y., Akiyama, A., & Kikuchi, Y.(2007, June). Pedestrian kinematics investigation with finite element dummy model based on anthropometry scaling method. In *Proceedings of the 20th International Technical Conference on the Enhanced Safety of Vehicles Conference,* Lyon, France, June 18-21, 2007..

Yoganandan, N., Arun, M. W. J., & Pintar, F. A. (2014). Normalizing and scaling of data to derive human response corridors from impact tests. *Journal of biomechanics, 47*, no. 8: 1749-1756.

DOT HS 812 641
May 2019

U.S. Department
of Transportation

**National Highway
Traffic Safety
Administration**

13859-051019-v3